Chapter 4
Synthesis and Application of Solution-Based II–VI and IV–VI Semiconductor Nanowires

Pornthip Tongying, Maksym Zhukovskyi and Masaru Kuno

Abstract Semiconductor nanowires (NWs) possess unique optical and electrical properties due to their anisotropic shape as well as their size-tunable electronic structure. In this chapter, we discuss the solution phase synthesis of II–VI and IV–VI semiconductor nanowires (e.g. ZnSe, CdS, CdSe, CdTe, PbS, PbSe, and $PbSe_xS_{1-x}$) as well as NW-based heterostructures involving core/shell and metal nanoparticle-decorated morphologies. We subsequently discuss the application of these materials within the context of nanowire yarns, nanowire-functionalized cotton textiles, and renewable energy applications involving nanostructured solar cells and photocatalytic hydrogen generation.

4.1 Introduction

One-dimensional (1D) II–VI and IV–VI semiconductor nanowires possess distinct optical and electrical properties due to their two-dimensional (2D) confinement and anisotropic shape. These features make them desirable for use in various applications. As illustrations, II–VI NWs have been used in photodetectors [1–4], solar cells [5–9] and in photocatalytic applications [10, 11]. Likewise, IV–VI NWs, especially the lead chalcogenides, have been used in infrared photodetectors [12], thermoelectric devices [13, 14] and in field effect transistors (FETs) [15–17]. NWs can also serve as the foundation for heterostructures having specifically engineered properties. This high degree of applicability, possessed by NWs, has thus made them one of the most studied nanosystems to date.

P. Tongying · M. Zhukovskyi (✉) · M. Kuno (✉)
Department of Chemistry and Biochemistry, University of Notre Dame,
251 Nieuwland Science Hall, Notre Dame, IN 46556, USA
e-mail: mzhukovs@nd.edu

M. Kuno
e-mail: mkuno@nd.edu

Q. Li (ed.), *Anisotropic Nanomaterials*, NanoScience and Technology,
DOI 10.1007/978-3-319-18293-3_4

Numerous approaches exist for creating NWs. Well established techniques include Vapor-Liquid-Solid (VLS) [18], oriented attachment [19], Supercritical-Fluid-Liquid-Solid (SFLS) [20] and Solution-Liquid-Solid (SLS) growth [21]. In this chapter, we focus on the SLS growth of group II–VI and IV–VI semiconductor NWs and their core/shell and metal nanoparticle-decorated counterparts. We then describe their potential uses in various applications.

4.2 Synthesis of II–VI and IV–VI Nanowires (NWs)

4.2.1 Solution-Liquid-Solid (SLS) Growth

SLS growth was first developed by Trentler et al. in 1995 [21] and is the liquid phase analogue of traditional VLS growth. In Trentler's original study, crystalline InP, InAs and GaAs nanowhiskers were synthesized using In and Ga/In nanoparticle (NP) catalysts formed in situ by the decomposition of tri-*tert*-butylindane and gallane. Resulting whiskers possessed widths of 10–150 nm with complementary lengths up to several micrometers. Metallic In (or Ga/In) droplets were found at the tips of these fibers suggesting their seeded growth.

SLS, like VLS growth, employs molten metal nanoparticles to solubilize elements derived from the thermolysis of molecular precursors. Semiconductor nucleation occurs within "catalyst" NPs once they become supersaturated. This eventually leads to self-segregation of the semiconductor at the droplet/solvent interface and, in turn, initiates seeded NW growth. The deposition of additional material at the semiconductor/droplet interface extends the NW length with continued growth occurring until the droplet becomes depleted of precursors. NW diameter control is established through the choice of catalyst nanoparticle size. Consequently, when narrow diameter NPs are used, growth of NWs with radii within the confinement regime of a number of systems is possible. Unwanted radial growth is additionally suppressed by using surfactants in solution that bind to exposed NW surfaces. Figure 4.1 summarizes this general SLS growth scheme.

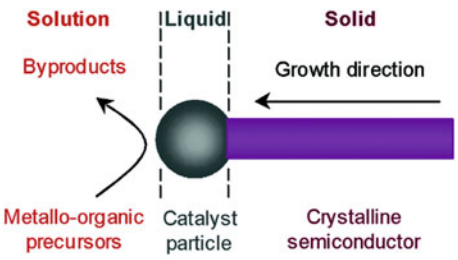

Fig. 4.1 Qualitative SLS growth mechanism for semiconductor NWs using low melting metal nanoparticle catalysts. Reprinted with permission from [34]. Copyright 2006 American Chemical Society

Although Trentler's early report showed proof-of-concept, resulting whiskers exhibited irregular morphologies as well as broad diameter and length distributions. This could be attributed, in part, to the uncontrolled size of employed metal NP catalysts. Consequently, the next stage in the development of SLS growth was the controlled synthesis of high quality metal NP catalysts with well-defined sizes and with narrow size distributions. Empirically, Bi has proven to be the best metal catalyst for producing high quality SLS NWs. This has motivated the various syntheses for size controlled Bi NPs described below.

In 2001, Yu et al. reported the formation of nearly monodisperse Bi, Sn and In NPs with controlled diameters using a heterogeneous seeded growth mechanism [22]. Specifically, NPs were formed by decomposing $Bi[N(SiMe_3)_2]_3$, $Sn(NMe_2)_2$, or $In(C_5H_5)$, in a solution containing Au NP seeds (diameter $\sim$1.5 nm) stabilized by a polymer [poly(styrene$_{0.86}$-co-vinyl-pyrrolidinone$_{0.14}$)]. Resulting NP diameters ranged from 7 to 25 nm. This work was followed by the development of a similar synthesis for d = 3–115 nm (d = 5–17 nm) Bi NPs involving the decomposition of $Bi[N(SiMe_3)_2]_3$ (or $BiCl_3$) in the presence of $Na[N(SiMe_3)_2]$ and poly(1-hexadecene)$_{0.67}$-co-(1-vinylpyrrolidinone)$_{0.33}$] [23]. Resulting NPs from these studies were subsequently used to grow InP and GaAs NWs with diameters in the range of 3.5–11 nm [24] and 6.0–17 nm [25]. Corresponding Bi NPs were used to demonstrate the growth of CdSe NWs with mean diameters ranging from 5 to 20 nm [26].

Grebinski et al. similarly reported the synthesis of Au/Bi core/shell NPs. This entailed coating small 1.5 nm diameter Au NPs with Bi through the decompositions of $Bi(Et)_3$ or $Bi(Bu)_3$ at low temperatures ($\sim$100 °C) in diphenyl ether [27]. The size of resulting NPs (d = 1.5–2.5 nm) was controlled through the amount of Bi precursor introduced. Using these particles, Grebinski subsequently demonstrated SLS-induced CdSe NW growth with diameters below 10 nm [27].

Later, Fanfair et al. reported the synthesis of Bi NPs through the $NaBH_4$ induced reduction of Bi(III) 2-ethylhexanoate in the presence of tri-*n*-octylphosphine (TOP) and dioctyl ether [28]. Resulting Bi NPs possessed an average diameter of 20 nm. This was followed by Li et al. who demonstrated a simple room temperature synthesis for Bi NPs involving the reduction of $Bi[N(SiMe_3)_2]_3$ or $BiCl_3$ with TOP in dioctyl ether [29]. Resulting Bi NPs were stabilized with amines such as oleylamine and had a mean diameter of $\sim$3.3 nm. These Bi NPs were subsequently used to demonstrate the growth of d = 7.9 and d = 22.3 nm CdSe NWs.

Finally, Puthussery et al. found that Bi NPs could be produced in situ through the exposure of $BiCl_3$ to chalcogen precursors being introduced into NW reaction mixtures [30]. Resulting Bi NP diameters were found to scale with $BiCl_3$ concentration and ultimately resulted in the development of facile "one pot" syntheses for CdS, CdSe and CdTe NWs.

In what follows, we describe details about the Bi-NP seeded growth of II–VI and IV–VI NWs.

4.2.1.1 Synthesis of Group II–VI NWs [CdE (E = S, Se, Te) and ZnE (E = Se, Te)]

The first synthesis of straight (d = 5–20 nm) CdSe NWs using Bi and Au/Bi NP seeded SLS growth was reported by Yu et al. in 2003 [26]. This was soon followed by Grebinski et al. who demonstrated the growth of d < 10 nm CdSe NWs using Au/Bi core/shell NPs [27]. The same group later reported the Au/Bi NP seeded growth of both straight and branched (d = 8–10 nm) CdSe and CdTe NWs [31, 32] as well as (d = 10.4 nm) CdS NWs [30]. Later, Li et al. reported the Bi NP seeded growth of straight CdSe NWs where a systematic variation of the reaction parameters (e.g. reaction temperature, precursor concentration and reaction time) led to wires with diameters ranging from d = 6 to 33 nm and with corresponding lengths up to tens of micrometers [33].

In the case of zinc chalcogenide NWs, Wang et al. first synthesized ZnTe NWs using Bi NPs in the presence of $Zn(stearate)_2$ (or diethylzinc, $ZnEt_2$) and tributylphosphine telluride (TBPTe) [34]. This was followed by the work of Dong et al. who produced $ZnSe_xTe_{1-x}$ NWs using Bi NPs in the presence of $Zn(stearate)_2$ and trioctylphosphine selenide (TOPSe)/TBPTe [35]. Resulting diameters were on the order of 10 nm with accompanying lengths of $\sim$1 μm. Fanfair et al. likewise showed the Bi NP seeded growth of branched ZnSe NWs using ZnO and TOPSe as precursors [36]. Resulting diameters were on the order of $\sim$10–40 nm with lengths on the micrometer scale. Finally, Petchsang et al. demonstrated the growth of ZnSe NWs using $Zn(stearate)_2$, TOPSe and $BiCl_3$ in tri-*n*-octylphosphine oxide (TOPO) [37]. The mean NW diameter was $\sim$22 nm with lengths on the order of 10 μm.

Chemicals involved in the synthesis of II–VI NWs generally include a group II metal source, a chalcogen precursor, a high boiling coordinating/non-coordinating solvent and a low melting metal NP catalyst. Furthermore, Bi is often the preferred catalyst since it empirically produces high quality wires. We now provide more details about the SLS growth of CdSe NWs since it has been the most extensively studied and developed SLS system to date.

4.2.1.2 Synthesis of CdSe NWs

For CdSe NWs, the group II precursor is often a metal salt [e.g. cadmium acetate ($CdAc_2$)] or a metal oxide [e.g. cadmium oxide (CdO)]. These metal salts/oxides, however, are not used directly. Instead, they are converted into intermediate species through exposure to long chain fatty acids such as octanoic, myristic or stearic acid. What results are species such as cadmium octanoate, cadmium myristate and cadmium stearate which are the actual cadmium precursors used in reactions and whose decomposition kinetics are controlled through the compound's corresponding ligand stability constant. This enables kinetic control of subsequent NW reactions and leads to the production of high quality wires.

Next, TOPSe, trioctylphosphine sulfide (TOPS) and trioctylphosphine telluride (TOPTe) are often employed as convenient chalcogen sources. They originate from

the work first done by Steigerwald [38] to find chemical routes for synthesizing bulk solid state materials. These convenient precursors are easily prepared by dissolving S, Se or Te powder in neat TOP, yielding TOPS, TOPSe or TOPTe stock solutions with concentrations in the ~1 M range. Such TOPX (X = S, Se, Te) precursors have since been used extensively in the chemical synthesis of analogous colloidal quantum dots [39].

Both coordinating (e.g. TOPO) and non-coordinating [e.g. octadecene (ODE)] growth solvents have been used in the SLS growth of CdSe NWs. These solvents serve two roles. First, they act as high boiling media that can sustain NW growth at elevated temperatures to improve their crystallinity. Common growth temperatures range from 240 to 360 °C. Next, coordinating solvents act as surface passivating agents during growth. This helps maintain optimal growth kinetics, prevents radial NW growth, and, in the case of surfactants such as TOPO, passivates surface-related NW defect states.

The experimental setup, which incorporates all of these elements, is shown in Fig. 4.2. In brief, growth solvents and precursors are combined in a three-neck flask. The flask is then connected to a Schlenk line. This allows the reaction vessel to be evacuated and backfilled with an inert gas such as nitrogen. A resistive heating mantle heats the precursors. Temperatures are controlled via a thermocouple connected to a temperature controller [40].

A more detailed description about the synthesis of CdSe NWs follows. First, CdO, TOPO and octanoic acid are mixed in a three neck flask. The mixture is then

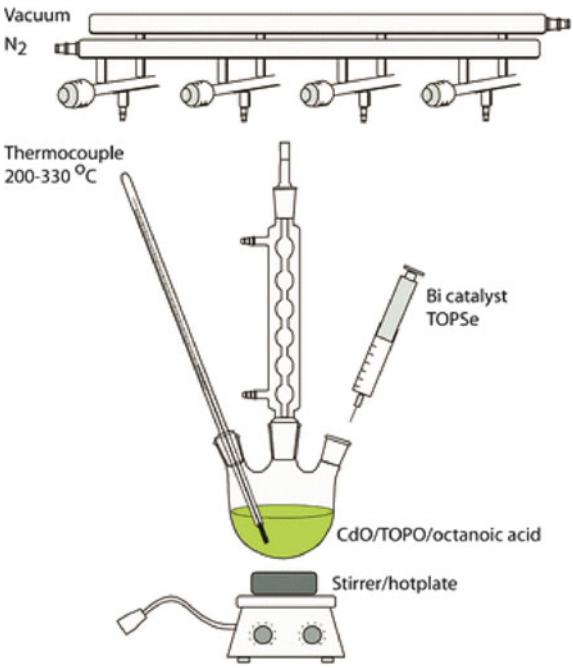

Fig. 4.2 Cartoon illustrating the reaction apparatus used for SLS NW growth. Chemicals and conditions represent those used in the synthesis of CdSe NWs [40]. Reproduced by permission of the PCCP Owner Societies

heated to melt the TOPO and is simultaneously degassed under vacuum to remove any water. Once complete, the temperature of the reaction mixture is raised to 320 °C under nitrogen. During this heating process, CdO reacts with octanoic acid to produce Cd(octanoate)$_2$. A color change of the solution from red to clear occurs highlighting this. Afterwards, the temperature is adjusted to the final growth temperature that typically ranges from 240 to 360 °C.

Once the reaction mixture temperature has stabilized, an injection solution consisting of TOPSe and Bi NPs (or $BiCl_3$) is introduced. An immediate color change from clear to brown occurs, indicating the nucleation and growth of CdSe NWs. The reaction mixture is then left heated at the growth temperature for several minutes whereafter it is cooled to room temperature. While still warm, the reaction mixture is diluted with toluene to prevent TOPO from solidifying. Produced NWs are recovered by centrifuging the resulting suspension. Subsequent washings steps are carried out to remove any excess surfactant where washing is done by exposing the wires to neat toluene and then centrifuging the suspension to recover the NWs. The obtained product is ultimately stored as a concentrated toluene suspension and remains stable for several years. Representative transmission electron microscopy (TEM) images of straight CdSe, CdTe and CdS NWs are shown in Fig. 4.3.

4.2.1.3 NW Diameter Control

In the SLS growth of CdSe and other NWs, diameter control is primarily achieved by preselecting the starting catalyst NP size. In this regard, a link between catalyst size and NW diameter has previously been established by Yu et al. who showed that in the case of CdSe NWs synthesized with Au/Bi (d = 8.72 nm) and Bi (d = 21 and 24 nm) NPs, resulting NWs had near identical diameters of 5–11 and 16–20 nm respectively [26]. A later study by Grebinski et al. showed that CdSe NWs made using d = 1.5–3.0 nm Au/Bi NPs had corresponding mean diameters which ranged from 7 to 10 nm and which increased with increasing Au/Bi NP size [31].

When $BiCl_3$ is used to produce NWs, diameter control is achieved by varying its concentration in the reaction mixture. Empirically, increasing $BiCl_3$ concentrations result in larger diameter Bi NPs as seen through increases in corresponding NW diameters. In the case of CdSe NWs, diameters have been tuned from d = 5 to 10.6 nm using a ten-fold increase in the amount of $BiCl_3$ added to reaction mixtures [30].

Apart from catalyst size, indirect ways exist for tuning NW diameters. In particular, varying the metal to chalcogen ratio of preparations influences NW diameters. Namely, larger NW diameters are obtained by increasing the Cd:Se ratio of SLS preparations [31]. Analogously, using more reactive metal/chalcogen precursors results in narrower diameter NWs. As an example, in the growth of ZnTe NWs, narrower wires were obtained when $ZnEt_2$ was used as a precursor over less reactive Zn(stearate)$_2$ under the same conditions [$ZnEt_2$: d = 3.7–5.0 nm; Zn (stearate)$_2$ d = 5–12 nm] [34].

Figure 4.4 shows resulting ensemble absorption and photoluminescence (PL) spectra of SLS grown CdSe NWs with varying mean diameters between 5 and

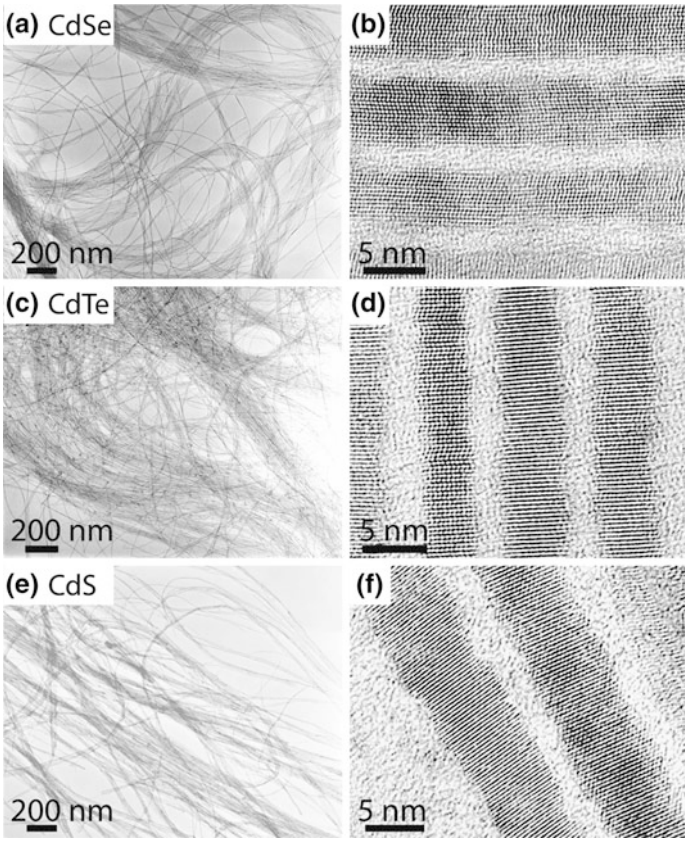

Fig. 4.3 Low and high magnification TEM images of straight **a**, **b** CdSe, **c**, **d** CdTe, and **e**, **f** CdS NWs. (Facile synthesis of II–VI nanowires using bismuth salts [30]. Copyright 2010 WILEY-VCH Verlag GmbH & Co. KGaA, Weinheim)

10.5 nm [30]. The spectra show that CdSe's band edge absorption and PL energies blueshift in tandem with decreasing NW diameter. This demonstrates the existence of carrier confinement effects and more broadly, highlights the ability of SLS growth to produce nanowires within the confinement regime of a number of important systems.

4.2.1.4 NW Branching

Next, despite the relatively low growth temperatures used in SLS growth, resulting wires are highly crystalline. However, many SLS-produced CdSe NWs exhibit mixtures of zincblende (ZB) and wurtzite (W) phases as well as twin boundaries [30, 31]. Interestingly, ZB/W phase admixtures have also been seen in VLS grown

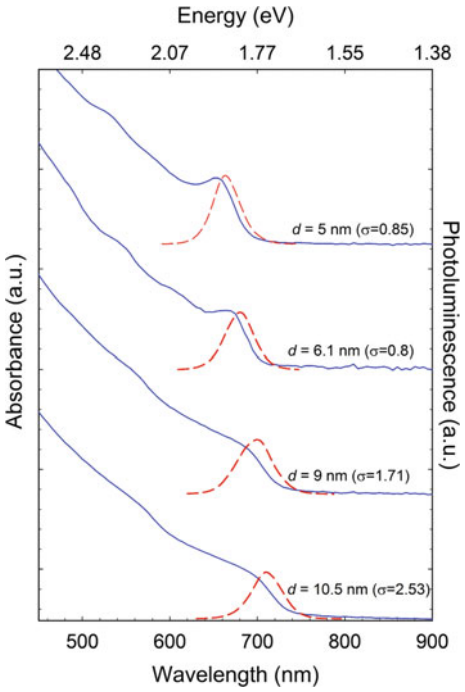

Fig. 4.4 Ensemble absorption (*solid blue line*) and PL (*dashed red line*) spectra of CdSe NWs with various diameters. (Facile synthesis of II–VI nanowires using bismuth salts [30]. Copyright 2010 WILEY-VCH Verlag GmbH & Co. KGaA, Weinheim)

GaAs, InAs and ZnSe NWs and occur when two crystal phases of similar energy exist [41, 42].

While such phase admixtures are not optimal for transport applications, other opportunities arise. Namely, phase admixtures can be used to control NW morphologies. This, in turn, enables the production of branched NWs. In the case of CdSe and CdTe NWs, what results are tripod, V-shaped and Y-shaped wires [31, 32]. Representative TEM images of branched CdSe NWs can be seen in Fig. 4.5.

The underlying origin of these branched morphologies results from the presence of a central ZB core at branching points of the wire. Exposed {111} faces then enable NW growth in different directions. This results in characteristic tripod, V-shape and Y-shape NW morphologies for II–VI NWs, first seen in Fig. 4.5 and outlined schematically in Fig. 4.6.

Branching is not unique to CdSe and CdTe NWs. It has also been seen in ZnSe [36] and PbSe NWs (discussed in the next section) [43]. Consequently, a general branching mechanism that rationalizes this phenomenon is discussed in detail in [40]. In brief, the simultaneous nucleation and growth of *two* NWs on a single catalyst NP (a geminate nucleation event) explains the various morphologies. Specifically, having two nucleated wires on a molten catalyst enables a common crystalline core to develop between the two wires. This core can subsequently lock the two arms into place along its unique crystallographic directions. For II–VI NWs such as CdSe and CdTe, a ZB core can thus unite two wires with orientations along

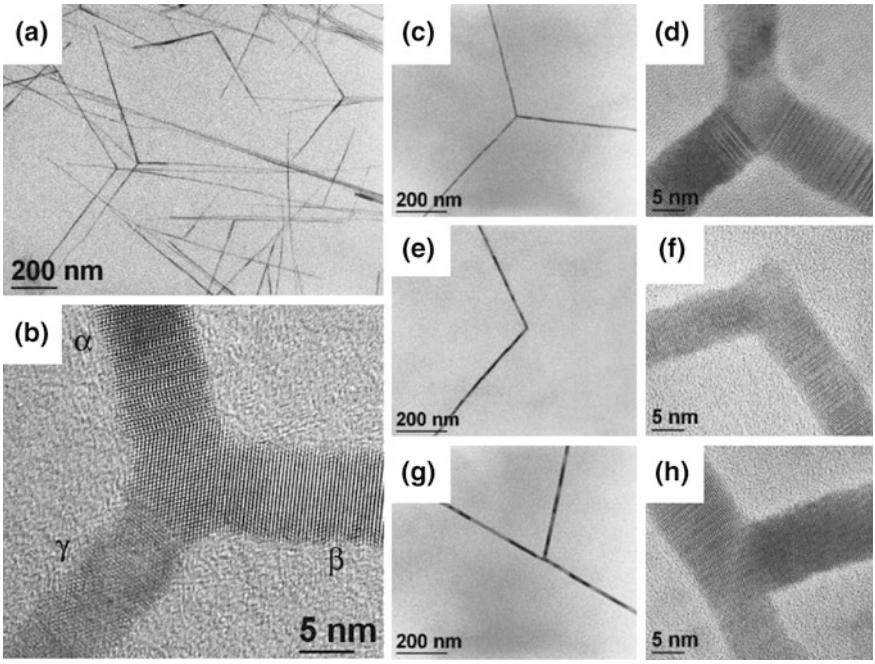

Fig. 4.5 **a** Low magnification TEM image of branched CdSe NWs. **b** High magnification TEM image of a tripod NW. Additional low and high magnification TEM images of **c**, **d** tripod, **e**, **f** V-shaped and **g**, **h** Y-shaped NWs. Adapted with permission from [31]. Copyright 2004 American Chemical Society

different ⟨111⟩ directions. At this point, if growth stops, a V-shaped NW results with a characteristic 109.5° angle. If growth continues through addition of material along a new {111} face of the ZB core, a tripod NW results. Alternatively, if growth continues through addition of material along an existing ⟨111⟩ direction, identical to that of one of the two arms, a Y-shaped NW results. In this manner, the appearance of tripod, V-shaped, Y-shaped and other branched CdSe/CdTe NW morphologies can be rationalized. An identical mechanism can be invoked to explain branching in lead chalcogenide wires described in the next section.

4.2.1.5 Synthesis of Group IV–VI NWs (PbS, PbSe, and $PbSe_xS_{1-x}$)

The flexibility of SLS growth enables not only II–VI but also IV–VI NWs to be synthesized [43–46]. Specifically, crystalline PbS and PbSe NWs have been made using Bi and Au/Bi NP seeded growth in tandem with lead oleate/TOPS [44] and lead acetate/TOPSe [43] precursor pairs. Specifically, PbSe NWs have been made by injecting a solution of TOPSe and Au/Bi NPs into TOP containing lead acetate and octanoic acid at 175 °C [43]. Resulting NWs possess mean diameters between

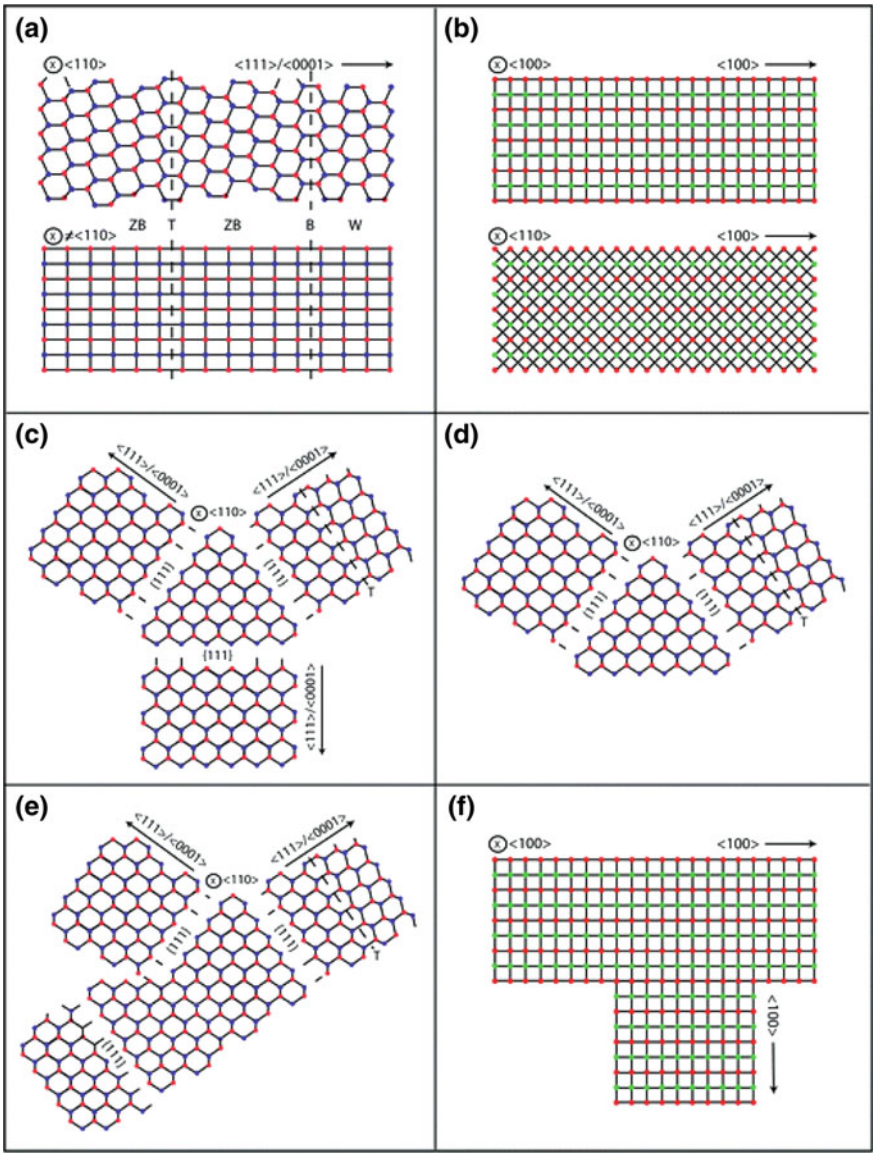

Fig. 4.6 Cartoon schematic of straight **a** CdSe or CdTe and **b** PbSe NWs. **c–e** Cartoon schematic of branched CdSe and CdTe NWs. **f** Cartoon schematic of T-shaped PbSe NWs [40]. Reproduced by permission of the PCCP Owner Societies

5 and 10 nm and have lengths ranging from 1 to 5 μm. In all cases, as with II–VI NWs, lead chalcogenide NW diameters are controlled by the size of the starting catalyst NP.

Branching has also been demonstrated with PbSe NWs despite the absence of a ZB/W phase admixture in this system [43]. In this regard, given that the rock salt crystal structure of PbSe is its only low energy crystallographic phase, only rock salt NWs are obtained. At first glance, this would not seem amenable to inducing branching. However, in practice, branched PbSe NWs with characteristic right angle and T-shapes have been produced [43]. The existence of these morphologies can again be rationalized using the above mentioned geminate NW nucleation mechanism described in the NW branching section of this chapter.

4.2.1.6 Use of Single Source Precursors

Due to the differing decomposition kinetics and/or reactivity of individual precursors, the use of metal/chalcogen precursor pairs has occasionally failed to produce highly crystalline and diameter controlled lead chalcogenide NWs [45]. Thus, to overcome this problem, single source precursors, where both metal and chalcogen exist within the same compound, have been employed. Specifically, Sun et al. have reported the synthesis of straight, diameter controlled PbS NWs using lead(II) diethyldithiocarbamate [$Pb(S_2CNEt_2)_2$] [45]. Binary PbS and PbSe as well as ternary $PbSe_xS_{1-x}$ NWs have also been made using lead(II) diethyldithiocarbamate [$Pb(S_2CNEt_2)_2$] or lead(II) imido(selenodiisopropylphosphinate) [$Pb((SeP^iPr_2)_2N)_2$] in the presence of $BiCl_3$ and TOPO [46]. In the latter study, resulting PbS and PbSe NWs possess a mean diameter of 9 nm with lengths exceeding 10 µm. Representative low and high magnification TEM images of these wires are shown in Fig. 4.7a–d.

The use of single source precursors simultaneously enables the growth of ternary alloy $PbSe_xS_{1-x}$ NWs. They are synthesized in an analogous manner to binary PbS and PbSe NWs through the decomposition of both $Pb((SeP^iPr_2)_2N)_2$ and $(Pb(S_2CNEt_2)_2$ in the presence of $BiCl_3$ [46]. Of note is that the NW composition can readily be tuned by varying the mole ratio of these two precursors. Specifically, $Pb((SeP^iPr_2)_2N)_2/Pb(S_2CNEt_2)_2$ mole ratios of 4:1, 1.5:1, 1:1, 1:1.5 and 1:4 yield ternary $PbSe_xS_{1-x}$ NWs where x = 0.8, 0.6, 0.5, 0.4 and 0.2, respectively. Resulting $PbSe_xS_{1-x}$ NW diameters range from d = 9 to 11 nm with corresponding lengths between 4 and 10 µm. The wires are fully alloyed with no apparent compositional gradients along their length. Representative low and high magnification TEM images of $PbSe_xS_{1-x}$ NWs are shown in Fig. 4.7e, f.

4.2.2 Synthesis of Core/Shell Semiconductor NWs

We now transition to a discussion about the growth of NW heterostructures, specifically, core/shell semiconductor NWs which possess a number of potentially useful properties given the presence of nanoscale heterojunctions [47]. In this section, we therefore describe how such core/shell morphologies can be synthesized, starting with the wires described in Sect. 4.2.1. In practice, this entails

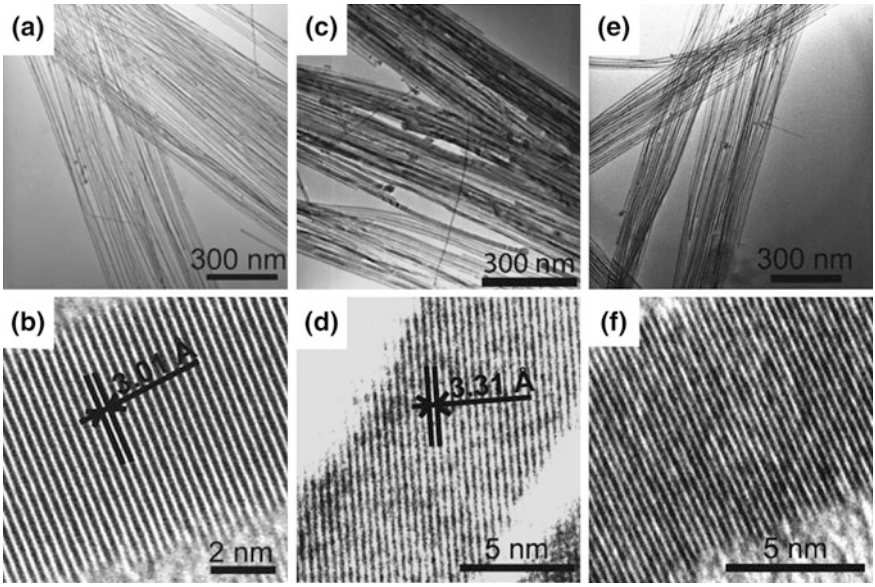

Fig. 4.7 Low and high magnification TEM images of binary **a**, **b** PbSe, **c**, **d** PbS and ternary **e**, **f** $PbSe_xS_{1-x}$ NWs. Adapted with permission from [46]. Copyright 2012 American Chemical Society

coating SLS-produced NWs with a second species through the slow introduction and thermolysis of molecular precursors.

Such core/shell structures generally involve Type I or Type II band offsets. In the former case, a Type I offset is created when the shell possesses a larger band gap than the NW core and when its conduction and valence bands simultaneously enclose those of the core. Consequently, upon photoexcitation of the core/shell structure, resulting carriers find themselves confined to the core. In principle, this leads to improved NW emission quantum yields (QYs), which stems from suppressed carrier access to surface states. For example, CdSe NWs coated with 6 and 10 monolayers CdS exhibit PL quantum which increase from 0.14 % (uncoated) to 0.25 and 0.46 %, respectively [48]. As will be discussed later in this chapter, photocatalytic hydrogen generation efficiencies also increase due to enhanced carrier lifetimes [10].

By contrast, Type II heterostructures possess staggered band offsets between core and shell conduction/valence bands. This means that one of the bands of the shell is higher in energy than that of the corresponding core. At the same time, the opposite is true of the other band. Representative systems include CdSe/ZnTe and CdS/ZnTe core/shell NWs.

The potential usefulness of such Type II heterostructures stems from their improved charge separation efficiencies upon photoexcitation [49, 50]. Specifically, because of the nature of the band offsets, carriers of one type are forced to stay in

the core while carriers of the other type experience favorable charge transfer into the shell. Consequently, Type-II heterostructures exhibit charge separation tendencies suitable for solar cell applications. Furthermore, these band offsets mean that tunable emission wavelengths in the red as well as infrared are possible if spatially indirect transitions in these materials can be realized [51]. Figure 4.8 shows SEM images of the various Type I and II core/shell NWs systems that have been made. Insets illustrate corresponding bulk core/shell band offsets.

The synthesis of these heterostructured NWs remains challenging due to the large parameter space that must be explored. This includes a consideration of the lattice mismatch between materials, the thermal stability of the parent NWs, the

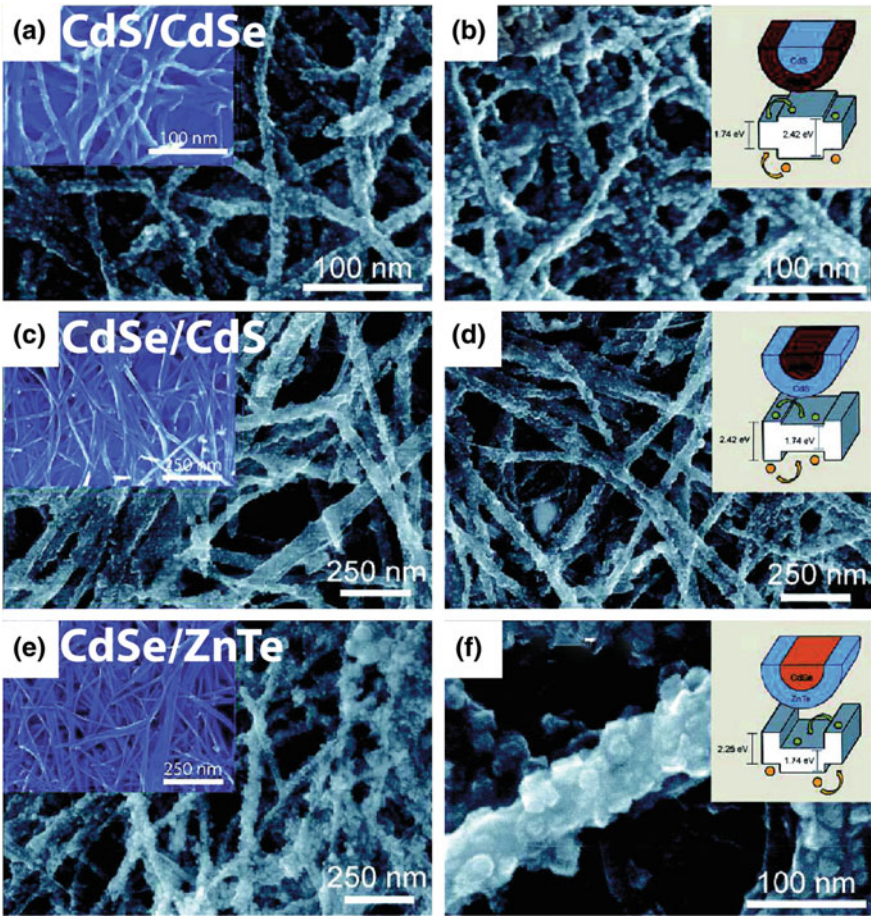

Fig. 4.8 SEM images of **a**, **b** CdS/CdSe, **c**, **d** CdSe/CdS and **e**, **f** CdSe/ZnTe core/shell NW heterostructures. *Insets* on the *right* illustrate bulk band offsets between the core and shell in each system. Reprinted with permission from [49]. Copyright 2008 American Chemical Society

selection of appropriate metal/chalcogen precursors for the shell, and the choice of a suitable growth solvent.

Having a small lattice mismatch between the NW and the shell makes more favorable the formation of core/shell structures. As an illustration, the 3.9 % lattice mismatch between CdSe and CdS makes the creation of CdSe/CdS or CdS/CdSe core/shell morphologies possible, as first demonstrated with colloidal CdSe quantum dots (QDs) [52]. Analogous CdSe/CdS NW heterostructures have since been realized [48, 49]. Similarly, CdSe/ZnTe NWs have been made by taking advantage of the 0.8 % lattice mismatch between CdSe and ZnTe [49]. Although a small lattice mismatch between the core and shell is generally preferred, a tolerance for larger mismatches exists. In the case of colloidal nanocrystals, CdSe/ZnS QDs have been made where the bulk lattice mismatch between CdSe and ZnS is 12 % [53, 54]. Likewise, in the case of NWs, ZnSe/CdSe NWs have been made with a 6.3 % lattice mismatch between materials [37].

At the same time, core NWs must remain stable at the elevated temperatures needed to thermalize shell precursors. Hence, the thermal stability of core NWs is important and is often tested by suspending them in a growth solvent and heating the suspension to temperatures compatible with the decomposition of the shell precursors. This has been discussed by Goebl et al. for CdSe and CdS NWs [49].

Optimal shell deposition temperatures, in turn, depend on the reactivity of the molecular precursors. For example, reactive precursor pairs such as dimethylcadmium ($CdMe_2$) and bis(trimethylsilyl)sulfide $(TMS)_2S$ [or bis(trimethylsilyl)selenide, $(TMS)_2Se$] thermalize at temperatures as low as 215 °C and lead to acceptable shell growth for CdSe (CdS) NWs. Replacing $(TMS)_2S$ [or $(TMS)_2Se$] with TOPS (or TOPSe), however, requires an increase in the deposition temperature in order to achieve suitable shell growth. This is due to the lesser reactivity of TOP-based precursors [49].

Finally, precursor introduction rates play an important role in determining the quality of resulting core/shell NWs. Specifically, slower injection rates result in smoother, more uniform coatings [49]. By contrast, rapidly introducing shell precursors often leads to uneven or patchy coatings.

4.2.2.1 Examples of Core/Shell NWs

Some examples of core/shell NWs include CdSe/CdS and CdSe/ZnS wires produced by Li et al. [48]. In this study, cadmium hexadecyl xanthate (Cd-HDX) and Zn-HDX single source precursors were used to achieve shell growth as well as different shell morphologies. Shell growth begins with the nucleation of CdS (or ZnS) on core CdSe NWs via the decomposition of Cd-HDX (or Zn-HDX) in TOP at 90 °C. This is then followed by a ripening process which ultimately results in ribbon formation along the core NW length, as illustrated in Fig. 4.9a [48].

CdSe/CdS NWs have likewise been made by decomposing $CdMe_2/(TMS)_2S$ [49] or $CdMe_2$/S powder [10] precursor pairs in a noncoordinating solvent such as squalane. Resulting shells appear rough and exhibit islanding (Fig. 4.8). Initial shell

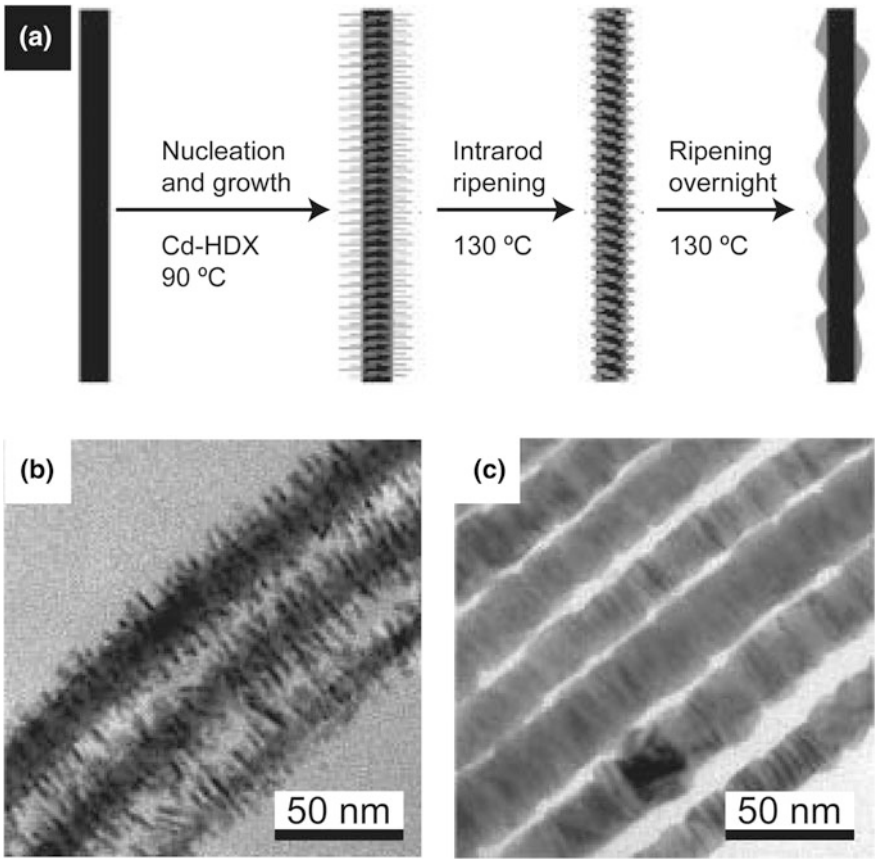

Fig. 4.9 **a** Schematic showing the growth of CdSe/CdS NWs. TEM images of **b** initial CdS nanorod formation on the surface of CdSe NWs and **c** the subsequent appearance of the shell after ripening. (Synthesis and characterization of colloidal core–shell semiconductor nanowires [48]. Copyright 2010 WILEY-VCH Verlag GmbH & Co. KGaA, Weinheim)

growth occurs through a Stranski-Krastanov growth mechanism, involving monolayer formation prior to island growth. This has also been observed for CdSe/ZnTe core/shell NWs. In the case of CdS/CdSe NWs, Volmer-Weber growth is observed where three-dimensional island growth is preferred from the beginning due to the unfavorable wetting of CdS with CdSe. In all cases, beyond these initial differences in shell growth, what results are thick polycrystalline shells, composed of randomly oriented nanocrystalline domains.

ZnSe/CdSe NWs have likewise been made by exposing ZnSe wires to $CdAc_2$ in TOPO at moderate temperature. TOPSe is subsequently introduced to initiate shell growth [37]. The procedure yields uniform shells where thicknesses can be varied by altering the reaction time after injection of the Se precursor. Representative TEM images of these core/shell NWs have been provided in Fig. 4.10.

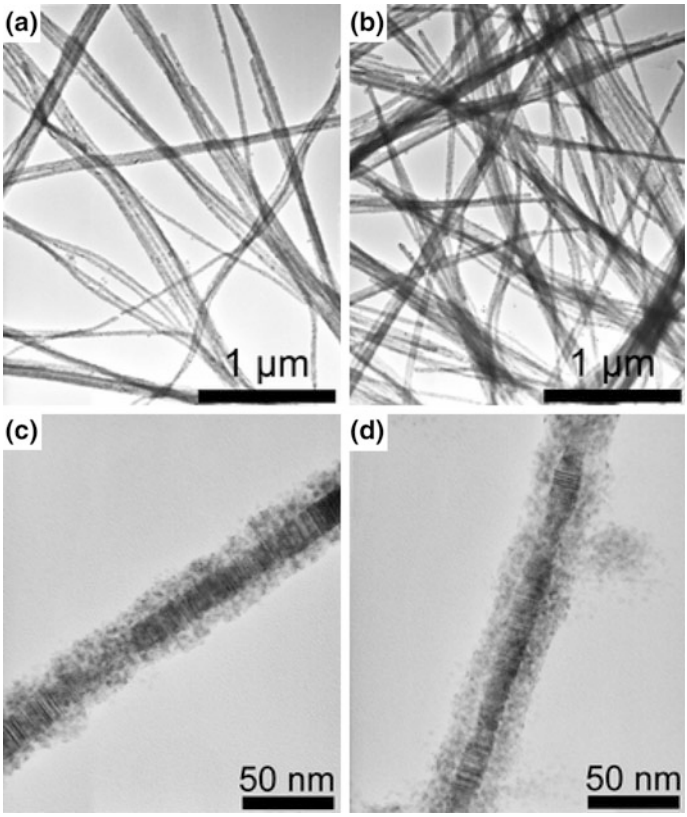

Fig. 4.10 Low and high magnification TEM images of ZnSe/CdSe NWs [37]. Reproduced by permission of The Royal Society of Chemistry

4.2.3 Hybrid Metal Nanoparticle Decorated NWs

Hybrid metal-semiconductor nanostructures result from combining two or more disparate metal and semiconductors into one system. Such heterostructures are multifunctional, making them useful in optoelectronic and photocatalytic applications [55–57]. As examples, decorating semiconductor nanostructures with metal nanoparticles has led to improved semiconductor charge separation efficiencies. This stems from photogenerated electrons preferentially migrating into metal nanoparticles, leaving behind holes in the semiconductor. Such enhanced charge transfer has been observed in CdSe NWs decorated with surface adsorbed Pt NPs [11]. Additionally, NW optical properties can be influenced by the presence of these particles. As an example, the presence of metal NP plasmon resonances has led to the observation of emission enhancement in Au NP decorated CdS NWs [58].

In what follows, we discuss the synthesis and growth of such hybrid metal-semiconductor NWs. This task of combining two or more dissimilar materials into

one nanostructured system is challenging. As described in Sect. 4.2.2 on the synthesis of core/shell nanowires, a numbers of parameters must be considered simultaneously in order to carry out such syntheses successfully. This includes a consideration of lattice constant mismatches between materials, the interfacial energy among materials, the presence of surface defects, and the accessibility/reactivity of the surface.

The energetics of the reaction also play a crucial factor in determining the growth of metal NPs onto NW surfaces. Fortunately, spontaneous nucleation of metal nanoparticles in the absence of elevated temperature or reducing agents is suppressed by the large barrier for homogeneous nucleation. Correspondingly, the deposition of metal NPs onto NW surfaces is aided by the lower barrier for heterogeneous nucleation [59, 60].

4.2.3.1 Examples of Hybrid Metal Nanoparticle Decorated Semiconductor NWs

We now illustrate several examples where metal NPs have been deposited onto the surfaces of solution-grown NWs. An initial example comes from Talapin et al. where Au NPs have been preferentially deposited onto the edges of zig-zag PbSe NWs by exposing them to $HAuCl_4$ in the presence of oleic acid and oleylamine at 35 °C (Fig. 4.11e) [61]. The decoration density is variable and can be further increased by

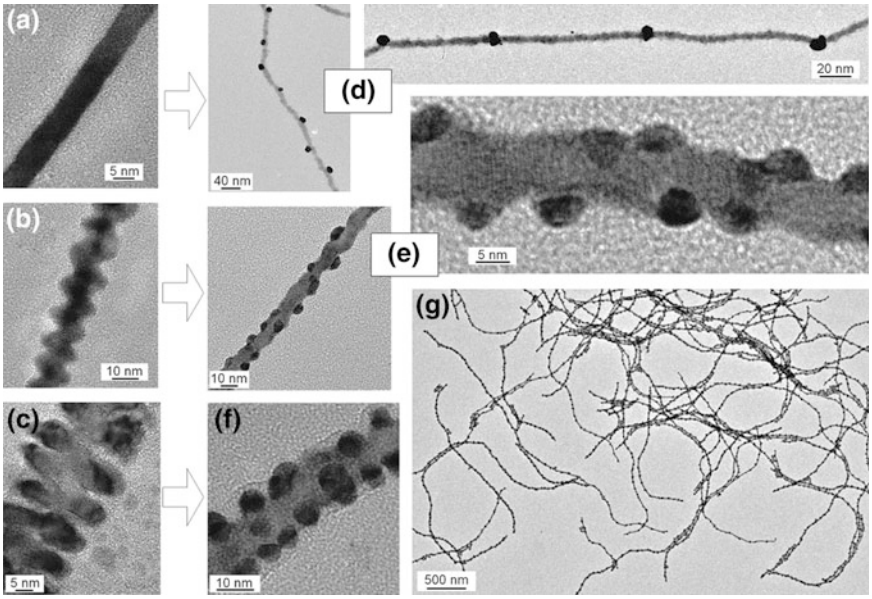

Fig. 4.11 TEM images of PbSe NWs with **a** straight, **b** zig-zag and **c** branched morphologies. TEM images of Au NP decorated **d** straight, **e** zig-zag and **f** branched PbSe NWs. **g** low magnification TEM images of Au NP decorated PbSe NWs. Reprinted with permission from [61]. Copyright 2007 American Chemical Society

using PbSe NWs with branched morphologies. This results in NW surfaces that are almost entirely covered with 5 nm Au NPs (Fig. 4.11f). Notably, NPs preferentially nucleate at the edges and branches of wires due to their higher surface energies.

Talapin et al. have similarly demonstrated the deposition of Au NPs onto straight PbSe NWs [61]. Resulting NWs show nearly equidistant Au NPs across the NW surface with a mean inter-particle spacing of 40–60 nm (Fig. 4.11d). Nucleation and growth in this case is non-selective given that straight NWs lack topological features that can serve as distinct nucleation sites.

Jen-La Plante et al. have likewise reported decorating straight CdSe NWs with Au NPs by adding a solution of gold chloride ($AuCl_3$), didodecyldimethylammonium bromide (DDAB, a phase transfer agent) and dodecylamine (DDA, a reducing agent) to a suspension of NWs. This results in Au NP nucleation and growth along the NW length [62]. Finally, Tongying et al. have successfully decorated CdSe and CdSe/CdS core/shell NWs with nanometer-sized Au NPs [10] using a procedure adapted from Menagen et al. [63]. In this study, a solution of $AuCl_3$ was added to a suspension of CdSe and CdSe/CdS core/shell NWs under vigorous stirring and under simultaneous UV illumination. Subsequent deposition of uniform d = 3–5 nm Au NPs was observed along the NW length within an extremely short period of time ($\sim$30 s). Images of these Au NP decorated wires are shown in Fig. 4.12.

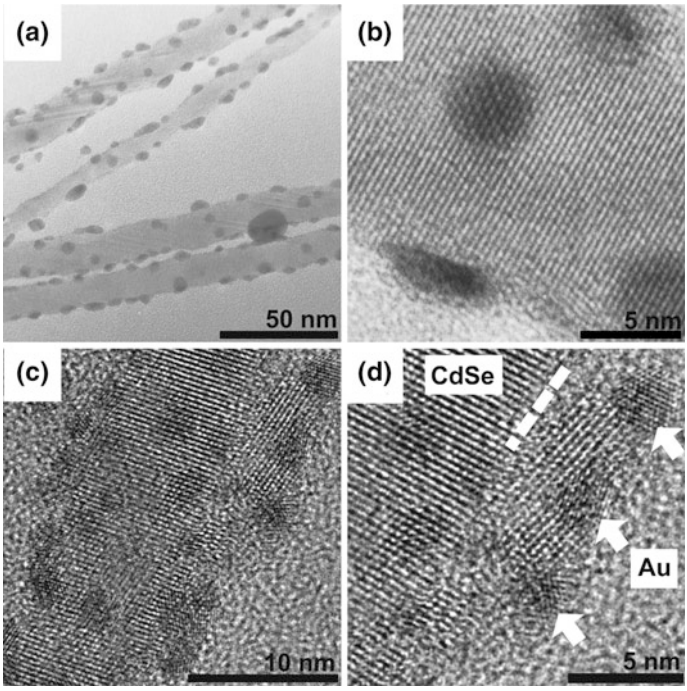

Fig. 4.12 Low and high magnification TEM images of Au NP decorated **a**, **b** CdSe **c**, **d** CdSe/CdS core/shell NWs. Reprinted with permission from [10]. Copyright 2012 American Chemical Society

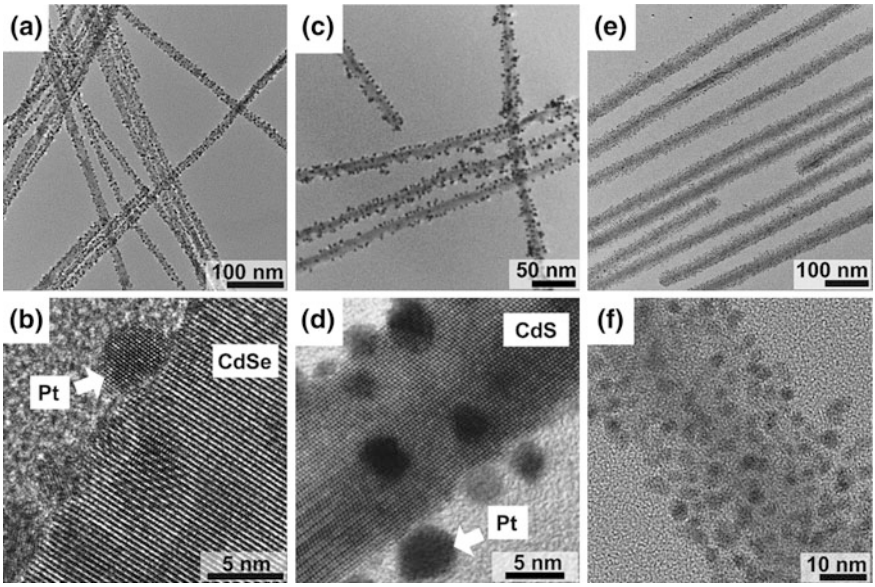

Fig. 4.13 Low and high magnification TEM images of Pt NP decorated **a**, **b** CdSe, **c**, **d** CdS and **e**, **f** CdSe/CdS core/shell NWs [11]. Adapted by permission of The Royal Society of Chemistry

In addition to Au, NWs can be functionalized with Pt NPs. This has been shown by Jen-La Plante et al. [62] for CdSe NWs as well as by Tongying et al. for CdSe and CdSe/CdS NWs [11]. In the latter case, CdSe and CdSe/CdS core/shell NWs were decorated with Pt NPs by modifying a procedure first developed for CdS NRs [64]. The synthesis entails exposing a suspension of NWs to platinum acetylacetonate in 1,2 dichlorobenzene. The mixture is then injected into a solution of oleic acid, oleylamine, and diphenyl ether at 200 °C to initiate NP growth. Pt NPs subsequently form along the NW length with resulting Pt NP sizes (diameter: 3–5 nm) controlled by the overall reaction time (5–7 min). Representative TEM images of these wires are shown in Fig. 4.13.

4.3 Applications of Semiconductor Nanowires

In Sect. 4.2 of this chapter we have discussed the SLS growth of NWs. We have also shown how NW morphologies can be altered by varying parameters such as the nature and concentration of precursors as well as the NP catalyst size. In addition, we have seen how NWs can be further modified by creating NW-based heterostructures. This includes core/shell morphologies as well as metal-semiconductor hybrid structures. In this section, we describe the assembly of solution-based NWs and their use in renewable energy application such as in photocatalytic hydrogen generation.

4.3.1 NW Assembly

The large carrier mobility, strong light absorbing nature, mechanical flexibility and high aspect ratio of semiconductor NWs make them suitable for a variety of electronic applications. Successful integration of NWs into devices, however, requires their assembly into mesoscopic structures. Towards this end, there have been many techniques which have been developed, including microfluidics [65], electrospinning [66], Langmuir–Blodgett [67], and magnetic/electric field alignment [68]. Unfortunately, many of these methods possess disadvantages including not being applicable to a wide range of semiconductors, not being scalable, and potentially resulting in the original nanostructure being affected through the use of additional chemicals (e.g. polymers, epoxides, amines etc.). The development of scalable NW assembly techniques is thus an important, ongoing research topic.

Manipulating NWs using electric fields represents one promising approach for their large-scale assembly. As an illustration, CdSe NWs have recently been aligned using AC dielectrophoresis (DEP) [1]. The approach entails depositing a suspension of NWs between two electrodes followed by the application of an AC electric field to align the wires. Figure 4.14a, b show bright field and PL images of resulting aligned CdSe NWs. Specifically, wires are seen to deposit onto both electrodes, orienting themselves along the field lines.

The origin of the AC DEP alignment effect stems from the interaction between induced dipoles in the wires and field gradients that exist at the electrode edges. Consequently, the DEP force and alignment velocity depend strongly on the

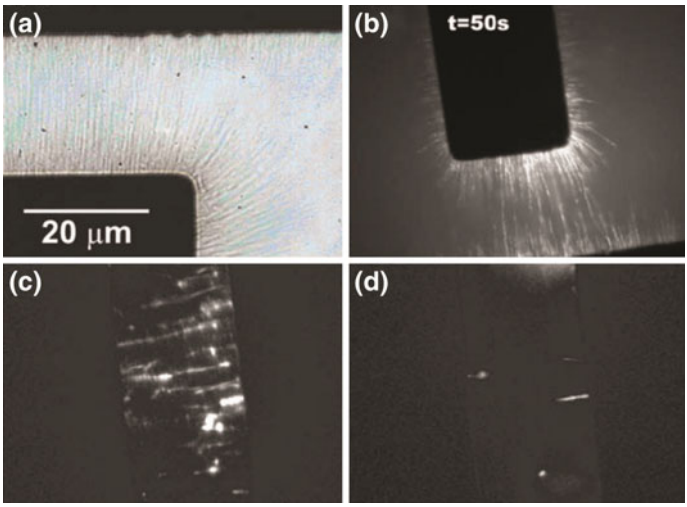

Fig. 4.14 AC DEP aligned CdSe NWs. **a** Bright field image after alignment. **b** Epifluorescence image taken at a given time during the alignment process. Emission images of CdSe NWs aligned **c** under illumination and **d** in the dark. Reprinted with permission from [1]. Copyright 2007, AIP Publishing LLC

magnitude of the induced dipoles in the wires. In this regard, an interesting observation made during these measurements was the enhancement of DEP alignment efficiency when CdSe NWs were illuminated with light. A hypothesis developed to explain this effect invoked the presence of mobile charges in the wires generated through above band gap illumination. Consequently, larger induced dipoles could result in the wires, leading to better overall NW alignment. Representative PL images comparing AC DEP aligned NWs under illumination and in the dark are shown in Fig. 4.14c, d.

The linear alignment of CdSe NWs results in a high degree of PL polarization anisotropy in both their absorption and emission. Figure 4.15a, b show representative photoluminescence images of aligned CdSe NW ensembles, which clearly demonstrate differences in the emission intensity with polarization angle. Furthermore, by defining an absorption/emission polarization anisotropy $\rho = (I_{\parallel} - I_{\perp})/(I_{\parallel} + I_{\perp})$ [$I_{\parallel}$ ($I_{\perp}$) is the observed emission intensity under parallel (perpendicular) polarized excitation relative to the aligned NW ensemble long axis] the degree of NW alignment can be quantified. These experiments reveal ρ-values of $\rho_{abs} = 0.24$ ($\rho_{em} = 0.27$) for aligned NW ensembles as well as $\rho_{abs} = 0.74$ ($\rho_{em} = 0.60$) for small NW bundles. When compared to ρ-values measured in individual NWs [$\rho_{abs} = 0.77$ ($\rho_{em} = 0.76$)], these ensemble ρ-values reveal the high degree of NW alignment achieved using AC DEP.

An analogous technique for organizing NWs into macroscopic yarns involves Light Induced Nanowire Assembly (LINA) [2]. The method entails slowly depositing a concentrated NW solution with a glass pipette onto the surface of a

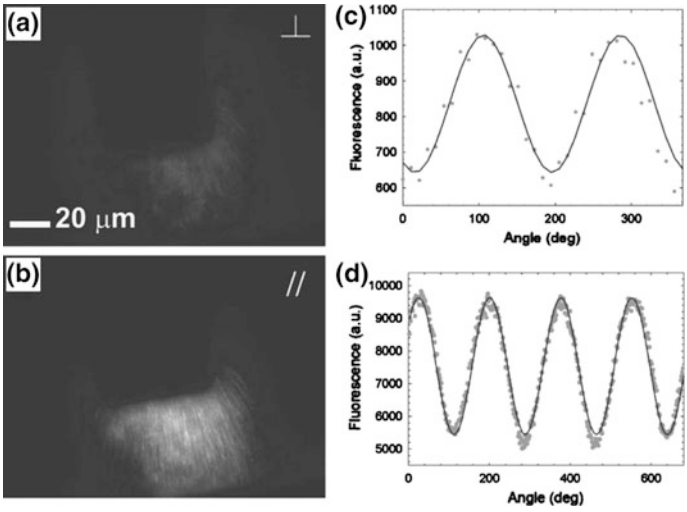

Fig. 4.15 **a** Perpendicular and **b** parallel polarized photoluminescence images of AC DEP aligned CdSe NW ensembles. Corresponding **c** absorption and **d** emission polarization anisotropy plots from an aligned ensemble. Reprinted with permission from [1]. Copyright 2007, AIP Publishing LLC

triboelectrically charged glass substrate under visible light illumination. A Van de Graaff generator (VDGG) charges the substrate prior to deposition. Experimentally, what results are NW fibers that spontaneously form, oriented normal to the substrate.

As with AC DEP, the approach exploits the interaction between induced dipoles in the wires and externally applied electric fields, in this case, stemming from charges on the substrate. Of note is that deliberately illuminating the sample with above band gap light creates many photogenerated carriers in the wires. This is aided by their large absorption cross sections [CdSe: $\sigma_{abs} \approx 6.93 \times 10^{-13}$ to $\sigma_{abs} \approx 3.91 \times 10^{-11}$ cm^2 μm^{-1} (d = 6–42 nm); CdTe: $\sigma_{abs} \approx 4.32 \times 10^{-13}$ to $\sigma_{abs} \approx 5.10 \times 10^{-12}$ cm^2 μm^{-1} (d = 7.5–11.5 nm)] [69–71] and leads to corresponding induced dipole moments of $\approx 10^5$ D assuming complete charge separation along the NW length [1]. Dipole-dipole interactions in solution then lead to end-to-end as well as side-to-side NW bundling and result in macroscopic NW bundles that consist of many wires aligned along the same direction. Figure 4.16 illustrates LINA conducted in toluene for three dilute CdSe, PbS and $PbSe_{0.5}S_{0.5}$ NW suspensions.

Next, Fig. 4.17a–e illustrates CdSe and CdTe NW yarns made using LINA. In this case, concentrated suspensions of the wires are slowly deposited onto a triboelectrically charged substrate under visible light illumination. Macroscopic NW alignment occurs whereupon subsequent solvent evaporation results in a NW yarn. Typical lengths are on the order of centimeters but yarns as long as 25 cm have been made. Corresponding diameters range from 10 to 20 μm and can be altered by changing the pulling rate from the NW suspension or by changing its concentration. In particular, increasing the pulling rate or alternatively, decreasing the NW stock concentration yields thinner yarns. Most importantly, LINA can be automated and enables the scalable formation of various NW yarns (Fig. 4.17f).

At the same time, LINA allows the creation of heterostructured yarns. For example, using a homogeneously mixed solution of CdSe and CdTe NWs results in a yarn made of both CdSe and CdTe NWs. Longitudinally segmented yarns made of different materials are also possible when LINA is carried out in a sequential fashion. This entails starting a yarn of one material followed by positioning the end of this yarn over a second charged substrate supporting a separate concentrated NW suspension. The second NW type subsequently adds to the end of the first yarn and extends it. Moving the resulting yarn back over the original substrate and repeating LINA then creates a segmented yarn of the form CdSe/CdTe/CdSe/CdTe etc.

In all cases, NW yarns show sizable optical polarization anisotropies. Specifically, CdSe NW yarns exhibit absorption polarization anisotropies of $\rho_{abs} \sim 0.2$ while homogenously mixed CdSe/CdTe yarns possess corresponding ρ-values of $\rho_{abs} \sim 0.13$. As with the earlier AC DEP results, this indicates that NWs in the yarns exhibit a relatively high degree of overall alignment. This opens up the possibility of using NW yarns in applications such as polarization-sensitive photodetectors [1, 2], a topic that will be discussed later in this chapter.

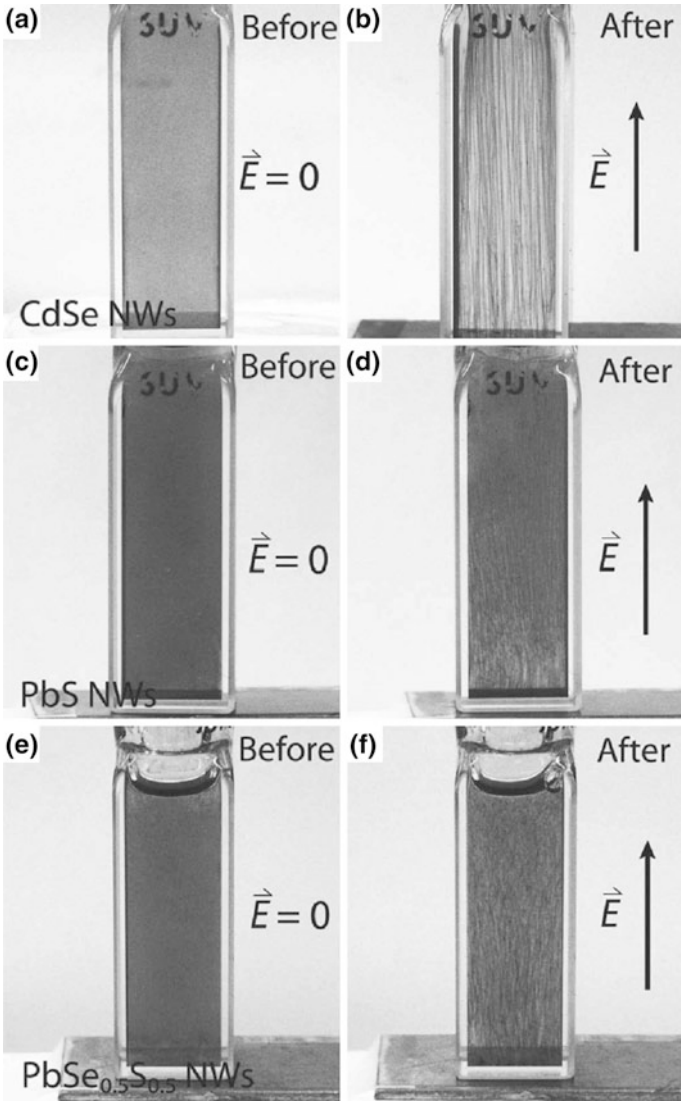

Fig. 4.16 **a**, **b** CdSe, **c**, **d** PbS, and **e**, **f** $PbSe_{0.5}S_{0.5}$ NW suspensions in toluene before and after LINA. (Light induced nanowire assembly: The electrostatic alignment of semiconductor nanowires into functional macroscopic yarns [2]. Copyright 2013 WILEY-VCH Verlag GmbH & Co. KGaA, Weinheim)

Finally, NWs can be used to functionalize natural fibers. In particular, cotton can be decorated with SLS grown NWs using the light or electrostatically-induced attraction of NWs [3]. What results are cotton fibers and textiles that retain their original mechanical properties while inheriting new chemical and optical properties from the deposited wires.

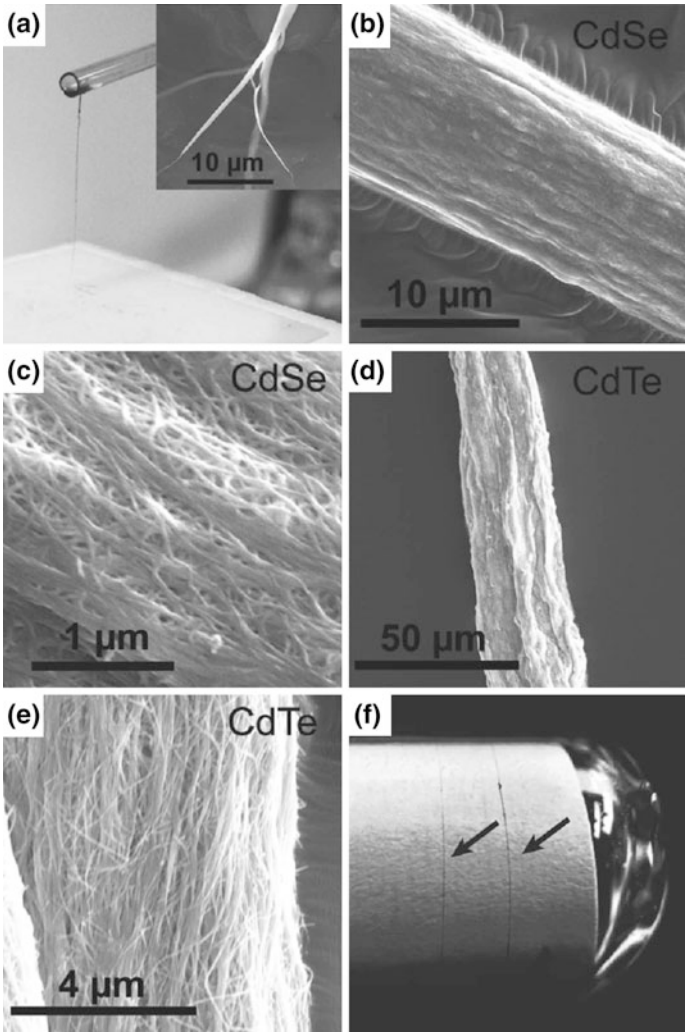

Fig. 4.17 **a** Image depicting NW yarn formation. SEM images of resulting **b**, **c** CdSe and **d**, **e** CdTe NW yarns. **f** 8 cm long CdSe NW yarn formed by automated pulling. (Light induced nanowire assembly: The electrostatic alignment of semiconductor nanowires into functional macroscopic yarns [2]. Copyright 2013 WILEY-VCH Verlag GmbH & Co. KGaA, Weinheim)

NW functionalization of cotton is carried out by dip-coating cotton fibers and textiles into NW suspensions under illumination with above band gap light. Alternatively, the cotton is charged with a VDGG prior to dip coating. The deposited NWs subsequently form an interlinked network that encapsulates individual cotton fibers in a conformal fashion (Fig. 4.18).

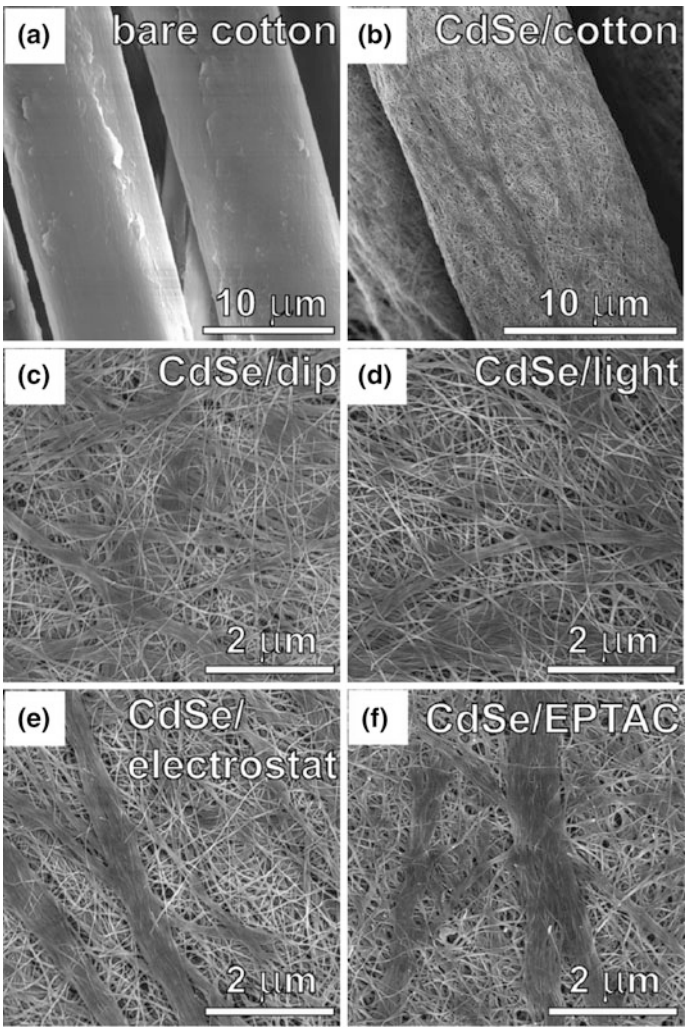

Fig. 4.18 SEM images of **a** bare cotton, and cotton functionalized with CdSe NWs after **b**, **c** simple dip-coating, **d** light-enhanced dip-coating, **e** VDGG-enhanced dip-coating and **f** dip-coating onto cationized cotton. Reprinted with permission from [3]. Copyright 2014 American Chemical Society

Illuminating NW suspensions with light during cotton functionalization results in an increased proclivity for depositing macroscopic NW bundles. As seen with LINA, the bundling phenomenon originates from the light-induced dipole-dipole interaction between individual wires. A bundling tendency is also observed when cotton is chemically cationized with 2,3-epoxypropyltrimethylammonium chloride (EPTAC) prior to dip-coating (Fig. 4.18f).

4.3.2 NW Barcodes

The ability to functionalize cotton with a wide variety of NWs as well as with binary combinations of NWs, enables the barcoding of textiles for identification purposes [3]. As shown in Fig. 4.19, the cotton/NW fabrics exhibit characteristic Raman spectra of component NWs. For illustration purposes, three NW combinations on cotton (i.e. CdTe/CdS, CdSe/CdS, CdTe/CdSe) have been tested. Consequently, combinations of NW types can lead to unique Raman signatures with potential uses in anti-counterfeiting and in other applications.

4.3.3 NW-Based Photodetectors

SLS-grown NWs have also been used to fabricate NW-based photodetectors [1–3]. In a first example, devices have been made using NW functionalized cotton fibers/textiles. Specifically, cotton/CdSe, cotton/CdTe and cotton/CdSe/CdTe threads were placed over two Au electrodes 60 μm apart. Under bias (−150 to 150 V) and

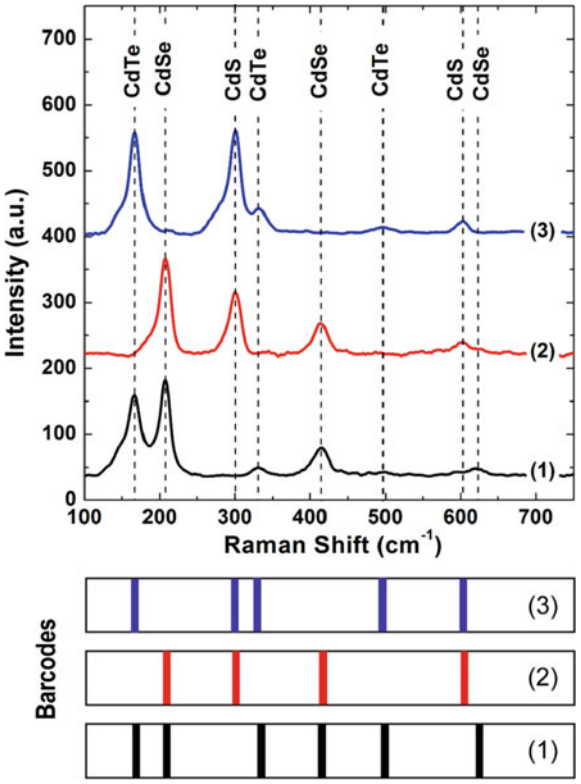

Fig. 4.19 Raman spectra of homogeneously mixed (*1*) cotton/CdSe/CdTe, (*2*) cotton/CdSe/CdS, and (*3*) cotton/CdTe/CdS NW fibers. Corresponding Raman barcodes obtained from each material are also shown. Reprinted with permission from [3]. Copyright 2014 American Chemical Society

under dark conditions, little current was observed. However, upon exposure to visible light the device current increased by more than two orders of magnitude. Figure 4.20a, shows typical current-voltage characteristics of these cotton/NW photodetectors in the dark and under illumination. Corresponding photocurrent action spectra of these cotton/CdSe and cotton/CdTe NW devices correlate with their linear absorption spectra. This indicates that the NWs are responsible for observed photocurrents in the devices (Fig. 4.20b). Similar results were observed for analogous NW (or NW yarn) based photodetectors [2, 4].

It was found that device responsivity could be improved by post-synthesis treatment of the NWs or by creating heterostructured NW networks (Fig. 4.20a, c). In the former case, NWs treated with pyridine to remove insulating species on the NW surface exhibited improved transport behavior across wires. In the latter case, NW mixtures composed of wires with Type II band offsets relative to each other yielded improved device charge separation efficiencies [50, 72]. Both approaches, in turn, resulted in corresponding enhancements of device responsivities.

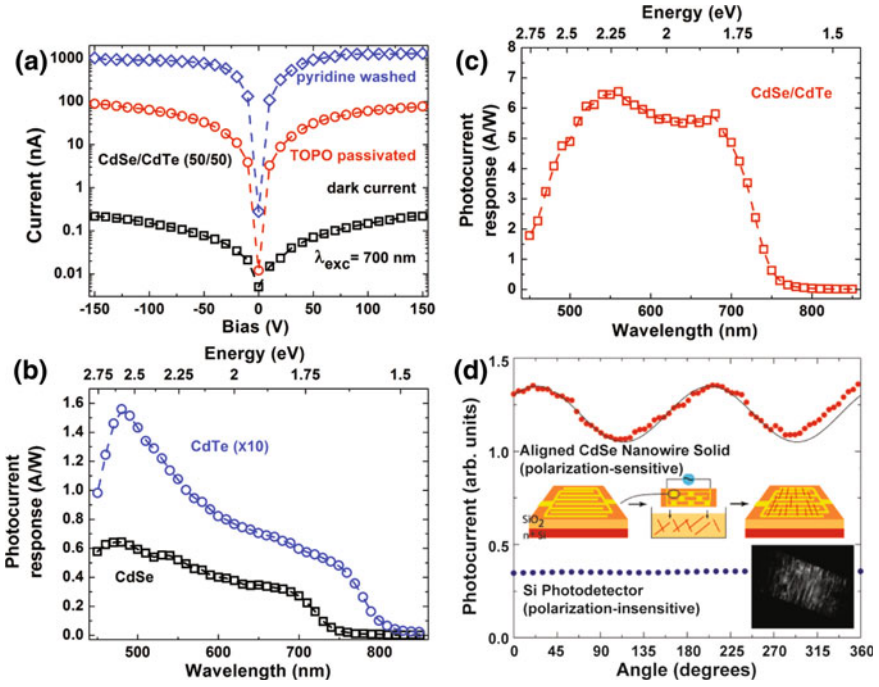

Fig. 4.20 **a** I–V characteristics and **b**, **c** photocurrent action spectra of CdSe, CdTe, and homogeneously mixed (50/50) CdSe/CdTe NWs deposited onto cotton fabrics. **d** Plot of the photocurrent polarization anisotropy from an aligned CdSe NW ensemble and comparison to the response of a commercial Si photodetector. **a**–**c** adapted with permission from [3]. Copyright 2014 American Chemical Society. **d** Adapted with permission from Singh [4]. Copyright 2007 American Chemical Society

Because NWs can be aligned using various techniques, resulting photodetectors are also polarization sensitive (Fig. 4.20d). In the case where AC DEP-aligned NWs have been used to make devices, corresponding photocurrent polarization anisotropies take values on the order of 0.13. This is similar to previously seen absorption (emission) anisotropy measurements of AC DEP-aligned NW ensembles ρ_{abs} = 0.24 (ρ_{em} = 0.27). They are also consistent with photocurrent polarization anisotropy measurements carried out on NW yarn photodetectors (ρ = 0.13–0.24) [1, 2]. The polarization sensitivity of NW photodetectors should be contrasted to the case of commercial Si photodetectors, which are not polarization sensitive.

4.3.4 NW Solar Cells

II–VI NWs are also potentially useful materials for creating nanostructured solar cells. Their anisotropic shape, favorable band gaps and large absorption cross sections make them useful active elements in solar cells. In this regard, there have been several recent demonstrations of solar cells built using SLS-produced NWs. A few examples are described below.

In a first study, Yu et al. demonstrated the use of CdSe NWs in a photoelectrochemical solar cell [8]. The device architecture consisted of indium tin oxide coated glass (ITO) as a transparent conductive substrate, a close packed NW absorber layer, sodium sulfide as an electrolyte and Pt as the counter electrode. The device also included colloidal CdSe quantum dots to fill in voids between NWs within the close packed NW absorber layer. The use of quantum dots made of the same material and possessing similar conduction and valence band levels was intended to improve the overall charge connectivity of the nanowire network. The energy level diagram illustrating the relative photoelectrochemical energies of different materials in the system is shown in Fig. 4.21a.

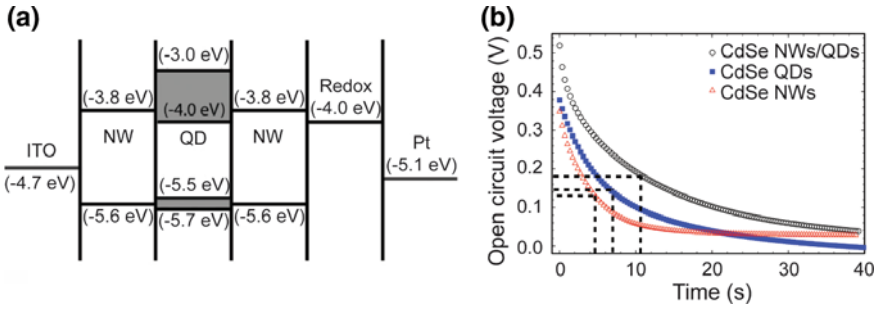

Fig. 4.21 **a** Energy level diagram and **b** open circuit voltage decays for photoelectrochemical solar cells system based on CdSe NWs and QDs. (A CdSe nanowire/quantum dot hybrid architecture for improving solar cell performance [8]. Copyright 2010 WILEY-VCH Verlag GmbH & Co. KGaA, Weinheim)

Experimentally, QD-modified NW solar cells show significant improvements in incident-photon-to-carrier conversion-efficiencies (IPCE) over comparable NW only cells. Values were seen to rise from 13 to 25 %. Furthermore, complementary open circuit voltage decay (OCVD) lifetimes increased from $t_{1/2}$ = 4.5 to 10.6 s (Fig. 4.21b). This demonstrated that QDs within the NW layer prevented back electron transfer to the electrolyte, enhancing overall charge separation efficiencies of the system. Consequently, device power conversion efficiencies were observed to rise from $\eta \sim 0.007$ to $\eta \sim 0.012$ % under simulated 1 sun conditions.

In a later example, CdSe NW solar cells were made using carbazole as a hole mediator [5]. Cells were built using fluorine doped tin oxide (FTO) coated glass as a conductive transparent substrate, ZnO as a compact (hole blocking) layer, a NW absorber layer, carbazole intercalated into the NW layer, sodium sulfide and sulfur as electrolytes and Cu_2S with reduced graphene oxide deposited on FTO as the counter electrode.

The purpose of the carbazole molecules was to achieve rapid hole extraction from the NWs, given their favorable HOMO level compared to the bulk CdSe valence band. Consequently, this would act to suppress unwanted charge recombination in the NWs following photoexcitation and would, in turn, improve device performance.

Figure 4.22a shows IPCE values recorded at different incident light wavelengths for CdSe NW devices with and without carbazole treatment. In the visible region of the spectrum, the maximum solar cell IPCE for untreated CdSe NWs was ~10 %. In the case of carbazole treated CdSe NWs, however, IPCE values were seen to rise up to ~45 %. Corresponding power conversion efficiencies also showed dramatic improvements from η = 0.01 % without carbazole to η = 0.46 % with carbazole. Complementary OCVD measurements confirm the effectiveness of charge separation in carbazole treated devices. Specifically, the apparent half-life of electrons in these solar cells increased from $t_{1/2}$ = 1.3 s without carbazole to 3.3 s with carbazole. This is illustrated in Fig. 4.22b.

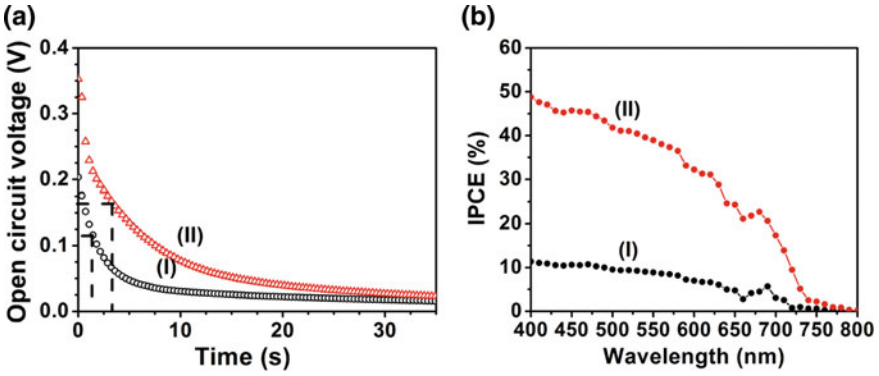

Fig. 4.22 **a** IPCE spectra and **b** open circuit voltage decays of solar cells based on CdSe NWs before (*I*) and after (*II*) carbazole treatment [5]. Reproduced by permission of The Royal Society of Chemistry

Along the same lines, Choi et al. used CdS NWs co-sensitized with squaraine dye to improve solar cell photoconversion efficiencies by extending their spectral response into the red and near infrared [7]. In this case, the organic dye was intended to act as an additional photosensitizer, adding to the absorption of NWs in the device. Choi's work subsequently showed that ~20 fold improvements in solar cell power conversion efficiencies were possible, from $\eta \sim 0.02$ to $\eta \sim 0.45$ %, using NW/squaraine composites.

Finally, Choi et al. explored using CdSe and CdS NW multilayers to improve solar cell performance [9]. The device consisted of FTO as an optically transparent substrate, ZnO as a blocking layer, stacked CdSe and CdS NW absorber layers, sodium sulfide and sulfur as electrolytes and reduced graphene oxide mixed with Cu_2S on FTO as the counter electrode. The underlying concept behind this solar cell was to exploit Type-II band offsets between CdSe and CdS NWs to achieve efficient charge separation following photoexcitation. Experimentally, multilayer CdSe and CdS cells were found to exhibit an order of magnitude improvement in power conversion efficiencies over comparable CdSe or CdS NW solar cells. Resulting power conversion efficiencies were $\eta \sim 1$ %.

4.3.5 NW-Based Photocatalysts for Hydrogen Generation

Semiconductor nanostructures with suitable band gaps ($E_g \sim 1.7$–3.1 eV) and electrochemical potentials ($E_{CB} \leq -0.41$ V and $E_{VB} \geq +0.82$ V vs. NHE at pH = 7) represent promising materials for use in photocatalytic hydrogen generation. This is because they absorb a good fraction of the incident solar radiation while their energetics enable charge transfer events that can carry out relevant chemistries. Furthermore, semiconductor nanostructures possess many advantages over their bulk counterparts due to their large surface-to-volume ratios, size-dependent optical properties, large absorption cross sections and ease of heterojunction fabrication.

On this last point, semiconductor nanostructures are interesting systems because of the relative ease of making heterojunctions with them. Implementing semiconductor/semiconductor heterointerfaces can dramatically improve not only the lifetime but also the spatial separation of photogenerated charges. Furthermore, nanostructures which feature metal/semiconductor heterojunctions should posses enhanced photocatalytic hydrogen generation activities since, in many cases, metal NPs possess suitable proton binding energies and simultaneously act as acceptors for photogenerated electrons.

We have previously illustrated in Sects. 4.2.2 and 4.2.3 how NW heterostructures can be made through the creation of core/shell morphologies as well as through the decoration of NWs with metal nanoparticles. Such NW-based heterostructures can, in turn, be used for photocatalytic hydrogen generation studies. Specific systems that have been investigated therefore include CdSe, CdSe/CdS core/shell, CdSe/Au NP, CdSe/Pt NP, CdSe/CdS/Au NP and CdSe/CdS/Pt NP NW photocatalysts. In all cases, UV-visible illumination of these photocatalysts in

aqueous solution and in the presence of sulfite/sulfide leads to hydrogen generation. Corresponding H_2 generation efficiencies have been quantified to better rationalize the role these semiconductor/semiconductor and metal/semiconductor heterojunctions play in dictating NW photocatalyst efficiencies.

Gas phase chromatography sampling of H_2 generation measurements generally reveal that CdSe NWs alone exhibit low H_2 generation efficiencies. Creating core/shell structures or decorating these NWs with metal nanoparticles, however, dramatically improves their H_2 generation efficiencies. Figure 4.23 shows specific results obtained from Pt NP decorated CdSe NW photocatalysts. Table 4.1 provides a fuller summary of observed hydrogen generation efficiencies across different CdSe NW systems.

Qualitatively, CdSe NWs show low H_2 generation efficiencies because of unwanted charge recombination processes in these wires. Table 4.1 shows that all other systems with semiconductor/semiconductor and metal/semiconductor junctions exhibit improved efficiencies. This indicates the importance of suppressing fast non-radiative processes in CdSe NWs or finding way to extract charges on timescales competitive with these events. Consequently, CdSe/CdS core/shell systems likely show enhancements due to improved carrier lifetimes stemming from the passivation of CdSe NW surface defects while metal NP decorated counterparts exhibit enhancements because of improved charge separation efficiencies.

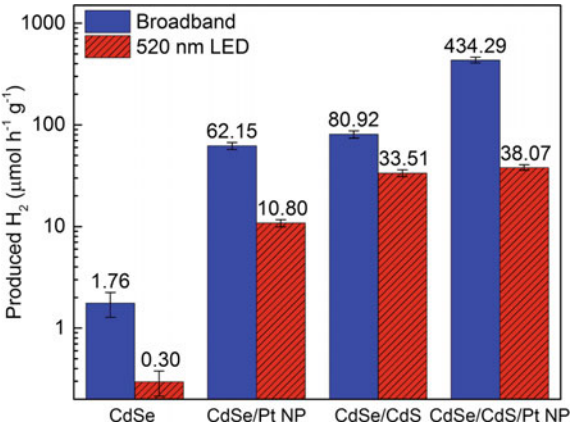

Fig. 4.23 Hydrogen generation efficiencies of CdSe NW-based photocatalysts [11]. Reproduced by permission of The Royal Society of Chemistry

Table 4.1 Summary of hydrogen generation efficiencies of CdSe NW-based photocatalysts under broadband and 520 nm illumination

NW system	Broadband illumination (μmol/h/g)	520 nm illumination (μmol/h/g)
CdSe	1.76, 1.98	0.30
CdSe/AuNP	2.61	
CdSe/CdS/Au NP	38.05	
CdSe/Pt NP	62.15	10.80
CdSe/CdS	58.06, 80.92	33.51
CdSe/CdS/Pt NP	434.29	38.07

To develop a more quantitative understanding of the results in Table 4.1 and why double heterojunction CdSe/CdS/Pt NP NWs show the largest H_2 generation efficiencies, transient differential absorption (TDA) experiments were conducted on each system. The technique enables one to follow the fate of photoexcited carriers in NWs following photoexcitation. In this regard, TDA spectroscopy is an important tool for probing the photophysics of semiconductor nanostructures because it allows one to spectroscopically follow the kinetics of excited carriers. For II–VI materials such as CdS and CdSe, observed TDA bleaches reflect the population of excited conduction band electrons given their relatively small effective mass [73]. Thus, by monitoring the temporal evolution of TDA bleaches, electron transfer reactions in II–VI nanostructures as well as their kinetics can be studied.

In what follows, only CdSe, CdSe/CdS and their Pt NP decorated counterparts are discussed. This is because the relatively poor performance of Au NP decorated systems ultimately stems from the slow electron discharge kinetics of Au, which inhibits reduction processes [74, 75]. Figure 4.24a first shows linear absorption spectra of CdSe, CdSe/CdS and CdSe/CdS/Pt NP NWs. Next the bottom of Fig. 4.24a shows experimental transient absorption bleaches observed after

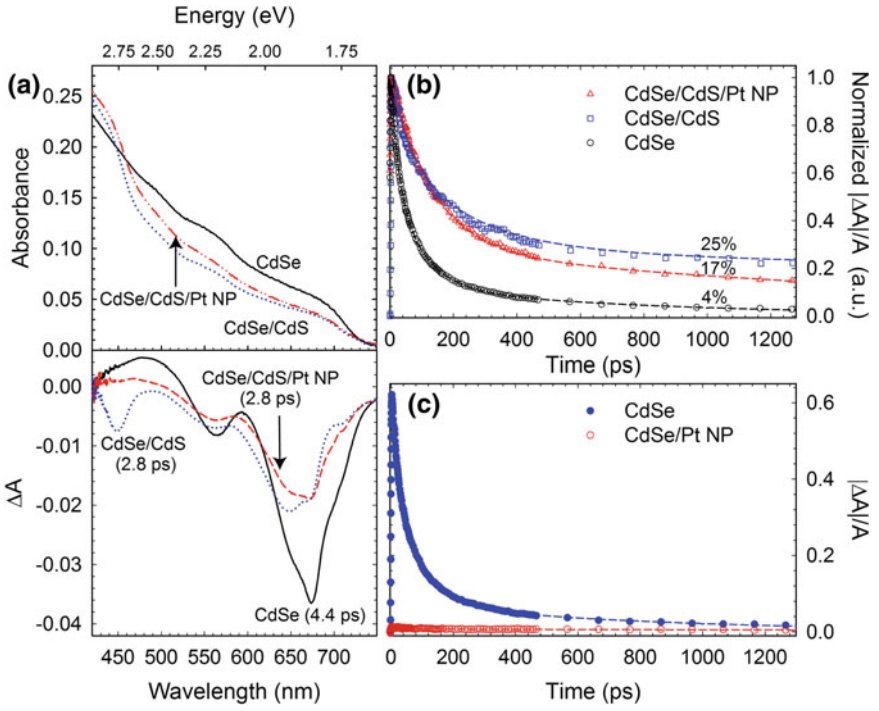

Fig. 4.24 **a** Linear absorption (*top panel*) and TDA (*bottom panel*) spectra of CdSe, CdSe/CdS and CdSe/CdS/Pt NP NWs. **b** Band edge bleach kinetics of CdSe, CdSe/CdS and CdSe/CdS/Pt NP NWs when excited at 387 nm. **c** Band edge bleach kinetics of CdSe and CdSe/Pt NP NWs when excited at 387 nm [11]. Reproduced by permission of The Royal Society of Chemistry

photoexciting each system. Negative going bleaches are seen at energies corresponding to features in the linear absorption and reflect the carrier population of different bands in the system. From the growth and decay kinetics of these bleaches, especially CdSe's band edge bleach at ~683 nm the kinetics of various electron transfer processes can subsequently be extracted.

In the case of CdSe NWs, Fig. 4.24b shows that their band edge bleach recovery occurs quickly within ~200 ps. This indicates that most of the photogenerated electrons in CdSe NWs recombine quickly in a non-radiative fashion due to the presence of defects on or within the wires. At 1 ns, only 4–8 % of the initially generated electrons remain wherein these long-lived species are most likely responsible for H_2 generation.

In the case of CdSe/CdS core/shell NWs, electron lifetimes noticeably increase due to the passivation of surface defects by the CdS shell. This has been observed directly in TDA measurements through increases in the remaining charge fraction at 1 ns when only the core of core/shell NWs has been excited [10, 11]. At 1 ns, between 25 and 33 % of the initially generated electrons remain available for chemical reduction, rationalizing why core/shell wires possess better H_2 generation efficiencies than their core only counterparts (Table 4.1).

In tandem, the Type-I heterojunction between the CdSe core and the CdS shell means that photogenerated electrons created in the shell also add to those in the core [10]. In the TDA measurement, this has been directly observed as a decrease of the CdS bleach at 450 nm accompanied by a growth of the CdSe bleach at 683 nm.

An interesting conclusion from these TDA measurements is that H_2 generation in CdSe/CdS core/shell NWs occurs not on the CdS shell but rather predominantly on the CdSe core [10]. This is because long-lived photogenerated electrons, responsible for the reduction, are seen to accumulate in the CdSe core. These H_2 generation results thus highlight the porosity of the CdS shell in CdSe/CdS NWs [10].

Next, in the case of Pt NP decorated systems, TDA measurements show ultrafast electron transfer into Pt. This can be seen in Fig. 4.24c where TDA kinetics of the CdSe band edge bleach show that the addition of Pt NPs causes an immediate (<1 ps) recovery of the band edge bleach. This ultrafast charge transfer, in turn, improves CdSe/Pt NP NW H_2 generation efficiencies since a larger fraction of CdSe's photogenerated electrons are transferred to Pt which possesses favorable proton binding affinities and electron discharge kinetics [74, 75], ultimately resulting in efficient H_2 generation.

Finally, in the case of Pt NP decorated CdSe/CdS NWs, the CdS shell passivates surface defects of the core. The CdS shell also contributes electrons to CdSe when excited. At the same time, the CdS shell contributes electrons to its surface adsorbed Pt NPs. Consequently, TDA measurements suggest a buildup of electrons in the CdSe core as well as in surface adsorbed Pt NPs when CdSe/CdS/Pt NP NWs are excited. This suggests that H_2 generation occurs in two places within this double heterojunction system—at the surface of the CdSe core and at the surface of the Pt NPs. The large H_2 generation efficiencies of this system (Table 4.1) can thus be rationalized as stemming from the combined effects of (i) the efficient surface passivation of CdSe NWs, which increases carrier lifetimes, (ii) the contribution of

additional electrons to the CdSe core from the CdS shell, which increases overall carrier densities, (iii) the efficient transfer of electrons from the CdS shell to surface adsorbed Pt NPs and (iv) the optimal proton binding affinities and electron discharge kinetics of Pt, which enable efficient proton reduction.

4.4 Conclusions and Outlook

In this chapter, we have discussed the synthesis of high quality semiconductor NWs using SLS growth. The method allows highly crystalline NWs to be grown at low temperatures. It also enables the growth of wires with tunable compositions, straight and branched morphologies and, more interestingly, the growth of wires within the confinement regime of a number of important systems. Various NW heterostructures can subsequently be fabricated using SLS-derived wires. This includes heterostructures exhibiting semiconductor/semiconductor and semiconductor/metal heterojunctions. Resulting NW architectures exhibit enhanced properties such as extended carrier lifetimes, improved emission quantum yields and enhanced charge separation efficiencies. The extent to which SLS NWs can be tuned, engineered, and assembled thus demonstrates their potential use within a broad range of applications. As illustrations, several examples, within the context of NW solar cells and photocatalysts, have been described.

Despite this great promise, however, challenges remain towards eventually implementing SLS-derived wires into commercial devices. This includes: (i) demonstrating scalable syntheses, (ii) developing a better understanding of NW surface defects so that their impact can be controlled and/or mitigated, (iii) developing high emission quantum yield NWs, (iv) improving the control of interfaces in heterostructured NWs, and (v) realizing the scalable, macroscopic assembly of these wires. Consequently, continued research and development on various fronts is needed, which portends exciting future developments for SLS NWs yet to come.

Acknowledgments PT thanks the Royal Thai Government Scholarship for financial support. MZ thanks the Notre Dame Innovation Postdoc Fund and ND Energy for financial support. MK thanks the NSF (CHE1208091) for financial support. We thank Rusha Chatterjee for assistance in editing this chapter.

References

1. R. Zhou, H.-C. Chang, V. Protasenko, M. Kuno, A.K. Singh, D. Jena, H.G. Xing, CdSe nanowires with illumination-enhanced conductivity: induced dipoles, dielectrophoretic assembly, and field-sensitive emission. J. Appl. Phys. **101**, 073704 (2007)
2. N. Petchsang, M.P. McDonald, L.E. Sinks, M. Kuno, Light induced nanowire assembly: the electrostatic alignment of semiconductor nanowires into functional macroscopic yarns. Adv. Mater. **25**, 601–605 (2013)

3. M. Zhukovskyi, L. Sanchez-Botero, M.P. McDonald, J. Hinestroza, M. Kuno, Nanowire-functionalized cotton textiles. ACS Appl. Mater. Interfaces **6**, 2262–2269 (2014)
4. A. Singh, X. Li, V. Protasenko, G. Galantai, M. Kuno, H.G. Xing, D. Jena, Polarization-sensitive nanowire photodetectors based on solution-synthesized CdSe quantum-wire solids. Nano Lett. **7**, 2999–3006 (2007)
5. H. Choi, M. Kuno, G.V. Hartland, P.V. Kamat, CdSe nanowire solar cells using carbazole as a surface modifier. J. Mater. Chem. A **1**, 5487–5491 (2013)
6. Z. Feng, Q. Zhang, L. Lin, H. Guo, J. Zhou, Z. Lin, ⟨0001⟩-Preferential growth of CdSe nanowires on conducting glass: template-free electrodeposition and application in photovoltaics. Chem. Mater. **22**, 2705–2710 (2010)
7. H. Choi, P.V. Kamat, CdS nanowire solar cells: dual role of squaraine dye as a sensitizer and a hole transporter. J. Phys. Chem. Lett. **4**, 3983–3991 (2013)
8. Y. Yu, P.V. Kamat, M. Kuno, A CdSe nanowire/quantum dot hybrid architecture for improving solar cell performance. Adv. Funct. Mater. **20**, 1464–1472 (2010)
9. H. Choi, J.G. Radich, P.V. Kamat, Sequentially layered CdSe/CdS nanowire architecture for improved nanowire solar cell performance. J. Phys. Chem. C **118**, 206–213 (2014)
10. P. Tongying, V.V. Plashnitsa, N. Petchsang, F. Vietmeyer, G.J. Ferraudi, G. Krylova, M. Kuno, Photocatalytic hydrogen generation efficiencies in one-dimensional CdSe heterostructures. J. Phys. Chem. Lett. **3**, 3234–3240 (2012)
11. P. Tongying, F. Vietmeyer, D. Aleksiuk, G.J. Ferraudi, G. Krylova, M. Kuno, Double heterojunction nanowire photocatalysts for hydrogen generation. Nanoscale **6**, 4117–4124 (2014)
12. Y. Yang, J. Li, H. Wu, E. Oh, D. Yu, Controlled ambipolar doping and gate voltage dependent carrier diffusion length in lead sulfide nanowires. Nano Lett. **12**, 5890–5896 (2012)
13. W. Liang, O. Rabin, A.I. Hochbaum, M. Fardy, M. Zhang, P. Yang, Thermoelectric properties of p-type PbSe nanowires. Nano Res. **2**, 394–399 (2009)
14. M. Fardy, A.I. Hochbaum, J. Goldberger, M.M. Zhang, P. Yang, Synthesis and thermoelectrical characterization of lead chalcogenide nanowires. Adv. Mater. **19**, 3047–3051 (2007)
15. R. Graham, C. Miller, E. Oh, D. Yu, Electric field dependent photocurrent decay length in single lead sulfide nanowire field effect transistors. Nano Lett. **11**, 717–722 (2011)
16. S.Y. Jang, Y.M. Song, H.S. Kim, Y.J. Cho, Y.S. Seo, G.B. Jung, C.-W. Lee, J. Park, M. Jung, J. Kim, B. Kim, J.-G. Kim, Y.-J. Kim, Three synthetic routes to single-crystalline PbS nanowires with controlled growth direction and their electrical transport properties. ACS Nano **4**, 2391–2401 (2010)
17. Y. Yang, X. Peng, D. Yu, High intensity induced photocurrent polarity switching in lead sulfide nanowire field effect transistors. Nanotechnology **25**, 195202 (2014)
18. R.S. Wagner, W.C. Ellis, Vapor-liquid-solid mechanism of single crystal growth. Appl. Phys. Lett. **4**, 89–90 (1964)
19. R.L. Penn, J.F. Banfield, Imperfect oriented attachment: dislocation generation in defect-free nanocrystals. Science **281**, 969–971 (1998)
20. J.D. Holmes, K.P. Johnston, R.C. Doty, B.A. Kogel, Control of thickness and orientation of solution-grown silicon nanowires. Science **287**, 1471–1473 (2000)
21. T.J. Trentler, K.M. Hickman, S.C. Goel, A.M. Viano, P.C. Gibbons, W.E. Buhro, Solution-liquid-solid growth of crystalline III-V semiconductors: an analogy to vapor-liquid-solid growth. Science **270**, 1791–1794 (1995)
22. H. Yu, P.C. Gibbons, K.F. Kelton, W.E. Buhro, Heterogeneous seeded growth: a potentially general synthesis of monodisperse metallic nanoparticles. J. Am. Chem. Soc. **123**, 9198–9199 (2001)
23. F. Wang, R. Tang, H. Yu, P.C. Gibbons, W.E. Buhro, Size- and shape-controlled synthesis of bismuth nanoparticles. Chem. Mater. **20**, 3656–3662 (2008)
24. H. Yu, J. Li, R.A. Loomis, L.-W. Wang, W.E. Buhro, Two- versus three-dimensional quantum confinement in indium phosphide wires and dots. Nat. Mater. **2**, 517–520 (2003)

25. H. Yu, W.E. Buhro, Solution–liquid–solid growth of soluble GaAs nanowires. Adv. Mater. **15**, 416–419 (2003)
26. H. Yu, J. Li, R.A. Loomis, P.C. Gibbons, L.-W. Wang, W.E. Buhro, Cadmium selenide quantum wires and the transition from 3D to 2D confinement. J. Am. Chem. Soc. **125**, 16168–16169 (2003)
27. J.W. Grebinski, K.L. Richter, J. Zhang, T.H. Kosel, M. Kuno, Synthesis and characterization of Au/Bi core/shell nanocrystals: a precursor toward II–VI nanowires. J. Phys. Chem. B **108**, 9745–9751 (2004)
28. D.D. Fanfair, B.A. Korgel, Bismuth nanocrystal-seeded III-V semiconductor nanowire synthesis. Cryst. Growth Des. **5**, 1971–1976 (2005)
29. Z. Li, A. Kornowski, A. Myalitsin, A. Mews, Formation and function of bismuth nanocatalysts for the solution–liquid–solid synthesis of CdSe nanowires. Small **4**, 1698–1702 (2008)
30. J. Puthussery, T.H. Kosel, M. Kuno, Facile synthesis and size control of II-VI nanowires using bismuth salts. Small **5**, 1112–1116 (2009)
31. J.W. Grebinski, K.L. Hull, J. Zhang, T.H. Kosel, M. Kuno, Solution-based straight and branched CdSe nanowires. Chem. Mater. **16**, 5260–5272 (2004)
32. M. Kuno, O. Ahmad, V. Protasenko, D. Bacinello, T.H. Kosel, Solution-based straight and branched CdTe nanowires. Chem. Mater. **18**, 5722–5732 (2006)
33. Z. Li, Ö. Kurtulus, N. Fu, Z. Wang, A. Kornowski, U. Pietsch, A. Mews, Controlled synthesis of CdSe nanowires by solution–liquid–solid method. Adv. Funct. Mater. **19**, 3650–3661 (2009)
34. F. Wang, A. Dong, J. Sun, R. Tang, H. Yu, W.E. Buhro, Solution–liquid–solid growth of semiconductor nanowires. Inorg. Chem. **45**, 7511–7521 (2006)
35. A. Dong, F. Wang, T.L. Daulton, W.E. Buhro, Solution–liquid–solid (SLS) growth of ZnSe–ZnTe quantum wires having axial heterojunctions. Nano Lett. **7**, 1308–1313 (2007)
36. D.D. Fanfair, B.A. Korgel, Twin-related branching of solution-grown ZnSe nanowires. Chem. Mater. **19**, 4943–4948 (2007)
37. N. Petchsang, L. Shapoval, F. Vietmeyer, Y. Yu, J.H. Hodak, I.M. Tang, T.H. Kosel, M. Kuno, Low temperature solution-phase growth of ZnSe and ZnSe/CdSe core/shell nanowires. Nanoscale **3**, 3145–3151 (2011)
38. M.L. Steigerwald, C.R. Sprinkle, Application of phosphine tellurides to the preparation of Group II-VI (2–16) semiconductor materials. Organometallics **7**, 245–246 (1988)
39. C.B. Murray, D.J. Norris, M.G. Bawendi, Synthesis and characterization of nearly monodisperse CdE (E = S, Se, Te) semiconductor nanocrystallites. J. Am. Chem. Soc. **115**, 8706–8715 (1993)
40. M. Kuno, An overview of solution-based semiconductor nanowires: synthesis and optical studies. Phys. Chem. Chem. Phys. **10**, 620–639 (2008)
41. M. Koguchi, H. Kakibayashi, M. Yazawa, K. Hiruma, T. Katsuyama, Crystal structure change of GaAs and InAs whiskers from zinc-blende to wurtzite type. Jpn. J. Appl. Phys. **31**, 2061–2065 (1992)
42. Q. Li, X. Gong, C. Wang, J. Wang, K. Ip, S. Hark, Size-dependent periodically twinned ZnSe nanowires. Adv. Mater. **16**, 1436–1440 (2004)
43. K.L. Hull, J.W. Grebinski, T.H. Kosel, M. Kuno, Induced branching in confined PbSe nanowires. Chem. Mater. **17**, 4416–4425 (2005)
44. K.-T. Yong, Y. Sahoo, K.R. Choudhury, M.T. Swihart, J.R. Minter, P.N. Prasad, Control of the morphology and size of PbS nanowires using gold nanoparticles. Chem. Mater. **18**, 5965–5972 (2006)
45. J. Sun, W.E. Buhro, The use of single-source precursors for the solution–liquid–solid growth of metal sulfide semiconductor nanowires. Angew. Chem. Int. Ed. **47**, 3215–3218 (2008)
46. A.C. Onicha, N. Petchsang, T.H. Kosel, M. Kuno, Controlled synthesis of compositionally tunable ternary $PbSe_xS_{1-x}$ as well as binary PbSe and PbS nanowires. ACS Nano **6**, 2833–2843 (2012)

47. J.K. Hyun, S. Zhang, L.J. Lauhon, Nanowire heterostructures. Annu. Rev. Mater. Res. **43**, 451–479 (2013)
48. Z. Li, X. Ma, Q. Sun, Z. Wang, J. Liu, Z. Zhu, S.Z. Qiao, S.C. Smith, G.M. Lu, A. Mews, Synthesis and characterization of colloidal core–shell semiconductor nanowires. Eur. J. Inorg. Chem. **27**, 4325–4331 (2010)
49. J.A. Goebl, R.W. Black, J. Puthussery, J. Giblin, T.H. Kosel, M. Kuno, Solution-based II–VI core/shell nanowire heterostructures. J. Am. Chem. Soc. **130**, 14822–14833 (2008)
50. S. Schäfer, A. Reich, Z. Wang, T. Kipp, A. Mews, Charge separation in CdSe/CdTe hetero-nanowires measured by electrostatic force microscopy. Appl. Phys. Lett. **100**, 022110 (2012)
51. S. Kim, B. Fisher, H.-J. Eisler, M. Bawendi, Type-II quantum dots: CdTe/CdSe(core/shell) and CdSe/ZnTe(core/shell) heterostructures. J. Am. Chem. Soc. **125**, 11466–11467 (2003)
52. X. Peng, M.C. Schlamp, A.V. Kadavanich, A.P. Alivisatos, Epitaxial growth of highly luminescent CdSe/CdS core/shell nanocrystals with photostability and electronic accessibility. J. Am. Chem. Soc. **119**, 7019–7029 (1997)
53. M.A. Hines, P. Guyot-Sionnest, Synthesis and characterization of strongly luminescing ZnS-capped CdSe nanocrystals. J. Phys. Chem. **100**, 468–471 (1996)
54. B.O. Dabbousi, J. Rodriguez-Viejo, F.V. Mikulec, J.R. Heine, H. Mattoussi, R. Ober, K.F. Jensen, M.G. Bawendi, (CdSe)ZnS core–shell quantum dots: synthesis and characterization of a size series of highly luminescent nanocrystallites. J. Phys. Chem. B **101**, 9463–9475 (1997)
55. R. Costi, A.E. Saunders, U. Banin, Colloidal hybrid nanostructures: a new type of functional materials. Angew. Chem. Int. Ed. **49**, 4878–4897 (2010)
56. A. Vaneski, A.S. Susha, J. Rodríguez-Fernández, M. Berr, F. Jäckel, J. Feldmann, A.L. Rogach, Hybrid colloidal heterostructures of anisotropic semiconductor nanocrystals decorated with noble metals: synthesis and function. Adv. Funct. Mater. **21**, 1547–1556 (2011)
57. U. Banin, Y. Ben-Shahar, K. Vinokurov, Hybrid semiconductor–metal nanoparticles: from architecture to function. Chem. Mater. **26**, 97–110 (2014)
58. P. Guo, J. Xu, X. Zhuang, W. Hu, X. Zhu, H. Zhou, L. Tang, A. Pan, Surface plasmon resonance enhanced band-edge emission of CdS–SiO_2 core–shell nanowires with gold nanoparticles attached. J. Mater. Chem. C **1**, 566–571 (2013)
59. X. Peng, J. Wickham, A.P. Alivisatos, Kinetics of II–VI and III–V colloidal semiconductor nanocrystal growth: "focusing" of size distributions. J. Am. Chem. Soc. **120**, 5343–5344 (1998)
60. D.V. Talapin, A.L. Rogach, M. Haase, H. Weller, Evolution of an ensemble of nanoparticles in a colloidal solution: theoretical study. J. Phys. Chem. B **105**, 12278–12285 (2001)
61. D.V. Talapin, H. Yu, E.V. Shevchenko, A. Lobo, C.B. Murray, Synthesis of colloidal PbSe/PbS core–shell nanowires and PbS/Au nanowire–nanocrystal heterostructures. J. Phys. Chem. C **111**, 14049–14054 (2007)
62. I. Jen-La Plante, S.E. Habas, B.D. Yuhas, D.J. Gargas, T. Mokari, Interfacing metal nanoparticles with semiconductor nanowires. Chem. Mater. **21**, 3662–3667 (2009)
63. G. Menagen, J.E. Macdonald, Y. Shemesh, I. Popov, U. Banin, Au growth on semiconductor nanorods: photoinduced versus thermal growth mechanisms. J. Am. Chem. Soc. **131**, 17406–17411 (2009)
64. S.E. Habas, P. Yang, T. Mokari, Selective growth of metal and binary metal tips on CdS nanorods. J. Am. Chem. Soc. **130**, 3294–3295 (2008)
65. Y. Huang, X. Duan, Q. Wei, C.M. Lieber, Directed assembly of one-dimensional nanostructures into functional networks. Science **291**, 630–633 (2001)
66. A. Theron, E. Zussman, A.L. Yarin, Electrostatic field-assisted alignment of electrospun nanofibres. Nanotechnology **12**, 384–390 (2001)
67. A. Tao, F. Kim, C. Hess, J. Goldberger, R. He, Y. Sun, Y. Xia, P. Yang, Langmuir–Blodgett silver nanowire monolayers for molecular sensing using surface-enhanced Raman spectroscopy. Nano Lett. **3**, 1229–1233 (2003)
68. S. Schäfer, Z. Wang, R. Zierold, T. Kipp, A. Mews, Laser-induced charge separation in CdSe nanowires. Nano Lett. **11**, 2672–2677 (2011)

69. J. Giblin, M. Syed, M.T. Banning, M. Kuno, G. Hartland, Experimental determination of single CdSe nanowire absorption cross sections through photothermal imaging. ACS Nano **4**, 358–364 (2010)
70. V. Protasenko, D. Bacinello, M. Kuno, Experimental determination of the absorption cross-section and molar extinction coefficient of CdSe and CdTe nanowires. J. Phys. Chem. B **110**, 25322–25331 (2006)
71. J. Giblin, M. Kuno, Nanostructure absorption: a comparative study of nanowire and colloidal quantum dot absorption cross sections. J. Phys. Chem. Lett. **1**, 3340–3348 (2010)
72. I. Gur, N.A. Fromer, M.L. Geier, A.P. Alivisatos, Air-stable all-inorganic nanocrystal solar cells processed from solution. Science **310**, 462–465 (2005)
73. V.I. Klimov, Optical nonlinearities and ultrafast carrier dynamics in semiconductor nanocrystals. J. Phys. Chem. B **104**, 6112–6123 (2000)
74. A. Wood, M. Giersig, P. Mulvaney, Fermi level equilibration in quantum dot–metal nanojunctions. J. Phys. Chem. B **105**, 8810–8815 (2001)
75. J.U. Bang, S.J. Lee, J.S. Jang, W. Choi, H. Song, Geometric effect of single or double metal-tipped CdSe nanorods on photocatalytic H_2 generation. J. Phys. Chem. Lett. **3**, 3781–3785 (2012)